

# FAST EMPIRICAL SCENARIOS

MICHAEL MULTERER, PAUL SCHNEIDER, AND ROHAN SEN

**ABSTRACT.** We seek to extract a small number of representative scenarios from large panel data that are consistent with sample moments. Among two novel algorithms, the first identifies scenarios that have not been observed before, and comes with a scenario-based representation of covariance matrices. The second proposal selects important data points from states of the world that have already realized, and are consistent with higher-order sample moment information. Both algorithms are efficient to compute and lend themselves to consistent scenario-based modeling and multi-dimensional numerical integration that can be used for interpretable decision-making under uncertainty. Extensive numerical benchmarking studies and an application in portfolio optimization favor the proposed algorithms.

## 1. INTRODUCTION

Multi-dimensional data in various fields require efficient processing for informed decision-making. In many practical applications, the moments of the sample realizations induced by the sample distribution, together with the sample realizations themselves, become central to inference tasks. For example, investors care not only about the variance of outcomes but also about the higher-order moments of the distribution of outcomes, in particular, about the possibility of extremely adverse outcomes. Similarly, in the case of estimating the stochastic discount factor (SDF) for asset pricing, one must ensure that it incorporates adequate information about the higher moments of the return distribution as it is important for modeling tail risk, see [Schneider and Trojani \[2015\]](#), [Almeida and Garcia \[2017\]](#), [Almeida et al. \[2022\]](#). As a result, portfolio optimization involving risky assets necessitates covariance matrices or even higher-order and/or non-linear functions of the moments, while the corresponding risk management is often scenario-based. The factor structure in interest rates also suggests a scenario-based approach, see [Engle et al. \[2017\]](#). More generally, the topic of summarizing information by replacing large samples of data with a small number of carefully weighted scenarios has found traction in many different communities, eg. scalable Bayesian statistics, see [Huggins et al. \[2016\]](#), clustering and optimization, see [Feldman et al. \[2020\]](#), etc. In the discipline of explainable artificial intelligence, the scenarios' probabilities can be used to define observation-specific explanations that give rise to a novel class of surrogate models, see [Ghidini et al. \[2024\]](#).

In this article, we are concerned with finding scenarios that exploit the availability of realizations from large samples of multi-dimensional data sets. The theoretical basis of our problem lies within the *truncated moment problem* (TMP), that underlies the theory of multivariate quadrature integration rules, see [Laurent \[2009\]](#), [Lasserre \[2010\]](#), [Schmüdgen \[2017\]](#). The TMP asks the question whether a finite sequence can be identified as the moment sequence of an underlying non-negative Borel measure, and if so, how to find another representing discrete measure (having finite support) with the smallest number of atoms that generates the same moment sequence. Keeping in mind data-driven applications, we introduce the concept of the *empirical moment problem* (EMP), in analogy to the TMP, in which moments are derived from the sample measure induced by the data. In particular, the EMP can be realized as a quadrature problem that aims to reduce the support set of the sample measure by choosing representative scenarios with the additional constraints of non-negativity and normalization of the corresponding weights.

**1.1. Related work.** Characterizing finite sequences as the moments of a non-negative Borel measure is the main idea behind the TMP and we refer to [Laurent \[2009\]](#), [Lasserre \[2010\]](#), [Schmüdgen \[2017\]](#) for a comprehensive discussion of the same. In particular, given a sequence of moments of a non-negative Borel measure, an algorithm is provided in [Lasserre \[2010\]](#), that seeks to extract the finite support of another representing measure that gives rise to the same sequence. In its prototypical form, it is akin to the

---

We gratefully acknowledge support from the SNF grant 100018\_189086 “Scenarios”.

multivariate Prony’s method, see [Kunis et al. \[2016\]](#). However, for practical purposes, especially for the EMP, Lasserre’s algorithm quickly becomes numerically and computationally demanding as the number of dimensions grows. Moreover, the number of extracted atoms is typically high. A linear programming approach is proposed by [Ryu and Boyd \[2014\]](#), which is also found to be numerically prohibitive for dimensions greater than three.

The EMP can also be formulated as a numerical quadrature problem, wherein the goal is to approximate

$$(1.1) \quad \int_{\Omega} h(\mathbf{x}) \, d\mu(\mathbf{x}) \approx \sum_{j=1}^m w_j h(\boldsymbol{\xi}_j),$$

for a given probability measure  $\mu$  on  $\Omega \subset \mathbb{R}^d$  by carefully choosing the *quadrature nodes*  $\boldsymbol{\xi}_1, \dots, \boldsymbol{\xi}_m$  and the corresponding *weights*  $w_1, \dots, w_m$ . Joint optimization of both the nodes and the weights, in general, corresponds to a non-convex problem, see [Oettershagen \[2017\]](#). Existing approaches take Monte Carlo samples of the nodes (if the underlying distribution is known and can be simulated from), and then find the optimal weights, that minimize a root mean squared quadrature error. In the quasi-Monte Carlo (QMC) literature, the nodes are chosen by deterministic, low-discrepancy sequences, that loosely translate to a “well-spread” set of nodes, and then choosing uniform weights, see [Sommariva and Vianello \[2009\]](#), [Bos et al. \[2011\]](#), [Bittante et al. \[2016\]](#), [Bos et al. \[2010\]](#).

With the assumption that  $h$  belongs to some *reproducing kernel Hilbert space* (RKHS)  $\mathcal{H}$  of functions with reproducing kernel  $\mathcal{K}$ , the worst-case quadrature error may be expressed using the reproducing property as, see [Oettershagen \[2017\]](#), [Bach \[2017\]](#),

$$(1.2) \quad \sup_{\|h\|_{\mathcal{H}} \leq 1} \left| \int_{\Omega} h(\mathbf{x}) \, d\mu(\mathbf{x}) - \sum_{j=1}^m w_j h(\boldsymbol{\xi}_j) \right| = \sup_{\|h\|_{\mathcal{H}} \leq 1} \left| \left\langle h, \int_{\Omega} \mathcal{K}(\mathbf{x}, \cdot) \, d\mu(\mathbf{x}) - \sum_{j=1}^m w_j \mathcal{K}(\boldsymbol{\xi}_j, \cdot) \right\rangle_{\mathcal{H}} \right| \\ \leq \left\| \int_{\Omega} \mathcal{K}(\mathbf{x}, \cdot) \, d\mu(\mathbf{x}) - \sum_{j=1}^m w_j \mathcal{K}(\boldsymbol{\xi}_j, \cdot) \right\|_{\mathcal{H}}$$

An approximation is obtained by choosing ideal candidates for the nodes and weights that minimize the right-hand side of the inequality (1.2). We note that the literature on kernel-based quadrature rules is extensive, and we list a few that are relevant to our problem. [Oettershagen \[2017\]](#) finds optimal weights given Monte Carlo nodes. [Bach \[2017\]](#), [Belhadji et al. \[2019\]](#), [Hayakawa et al. \[2022\]](#) choose nodes based on random designs, which are based on either a Mercer-based decomposition, see [Bach \[2017\]](#), or a Nyström approximation of the kernel.

Scattered data approximation, see [Wendland \[2005\]](#), [Fasshauer \[2007\]](#), is another field which is related to the EMP. The question is how to construct kernel interpolants that can approximate functions in the RKHS sufficiently well. Our proposal is closest in spirit to this literature, see [De Marchi and Schaback \[2010\]](#), [Pazouki and Schaback \[2011\]](#). [Cosentino et al. \[2020\]](#) and [Bouchot et al. \[2016\]](#) also provide algorithms that perform greedy subsampling of nodes from a set of samples.

**1.2. Contributions.** We propose two algorithms for scenario extraction, where the first one can be applied to both the TMP and the EMP, while the second one is suited solely for the EMP. The first algorithm produces scenarios with uniform weighting utilizing Householder reflections, specializing the TMP to the uniform measure. It is the fastest algorithm considered in this paper and reveals a set of uniformly distributed *covariance scenarios* whose moment sequence matches up perfectly with that of the sample measure up to second-order moments.

The second algorithm is designed for solving the EMP, wherein the goal is to choose a good representative set of  $m$  scenarios from a given set of  $N$  samples, that matches the polynomial moments of the data samples sufficiently well in the regime of  $m \ll N$ . In particular, we reduce the support set of the sample measure to produce a finite atomic probability measure that ensures both positivity and normalization of the atomic weights. There are several reasons why such convex specifications of the weights are preferable: the RKHS may be mis-specified if the weights are negative and also to maintain positivity of the integral operator  $h \mapsto \int h(\mathbf{x}) \, d\mu(\mathbf{x})$ , see [Hayakawa et al. \[2022\]](#). Furthermore, the normalization also helps us in assessing the relative importance of the scenarios in describing the sample moment information and can thus be used for generative modeling of the underlying data. The proposed algorithm offers a

computational solution to the data-dependent orthogonal matching pursuit in the RKHS as in [Pazouki and Schaback \[2011\]](#), and is hence referred to as *orthogonal matching pursuit* (OMP). It is based on the pivoted-Cholesky, see, e.g., [Harbrecht et al. \[2012\]](#), decomposition of the kernel matrix which exempts us from choosing the scenarios (or atoms of the reduced measure) using a Mercer expansion of the associated kernel of our proposed RKHS.

We demonstrate the robustness, computational efficiency, and adaptivity of the algorithm for large samples of multivariate data and contrast it with existing approaches in the literature. Furthermore, we demonstrate the capacity of the scenarios (extracted with only sample moment information) to capture tail risk as well. We show this in the context of portfolio optimization of panel data of asset returns with (non-smooth) expected shortfall constraint.

Finally, we prove that basis pursuit or LASSO, see [Hastie et al. \[2003\]](#), [Foucart and Rauhut \[2013\]](#), induced by  $\ell_1$ -regularized least squares, a standard approach in the literature on compressive sensing and machine learning, does not lend itself to recovering optimal quadrature rules in the context of the EMP. To the best of our knowledge, we provide the first result that shows the inadequacy of the LASSO in constructing quadrature rules from sample measures. As a consequence of this, first-order proximal algorithms cannot be used in this context either.

**1.3. Outline.** The remainder of this article is organized as follows. In [Section 2](#), we formally introduce the TMP and the notion of moment matrices, based on which we propose covariance scenarios. In [Section 3](#), we present the empirical version, the EMP, and reformulate the problem in an RKHS framework. In [Section 4](#), we propose the OMP algorithm, and demonstrate its applicability for the EMP. Moreover, we comment on why basis pursuit cannot work in the context of the EMP. [Section 5](#) addresses numerical experiments, where we benchmark our proposed algorithms against existing approaches. In [Section 6](#), we conclude and identify areas for future research.

## 2. THE TRUNCATED MOMENT PROBLEM

In this section, we review the key theoretical background of the TMP as the underlying mathematical foundation. Moreover, we make the connection of TMPs with quadrature rules in the multi-dimensional framework. Finally, we present a specialized algorithm for the direct extraction of scenarios from covariance matrices in a fast manner.

**2.1. Background.** Let  $\Omega \subset \mathbb{R}^d$  and  $\mathcal{B}$  denote the Borel  $\sigma$ -algebra on  $\Omega$ . Suppose that we are given a finite real sequence  $\mathbf{y} = (y_\alpha)_{|\alpha| \leq q}$  indexed by  $\alpha := (\alpha_1, \dots, \alpha_d) \in \mathbb{N}^d$  with  $|\alpha| := \alpha_1 + \dots + \alpha_d \leq q$ , where  $q \in \mathbb{N}$ . We say that  $\mathbf{y}$  has a *representing measure* if there exists a Borel measure  $\mu: \mathcal{B} \rightarrow [0, \infty)$  such that

$$(2.1) \quad y_\alpha = \int_{\Omega} \mathbf{x}^\alpha d\mu \quad \text{for } |\alpha| \leq q.$$

If [\(2.1\)](#) holds,  $\mathbf{y}$  is called a *truncated moment sequence* (TMS). The TMP asks: How to check if a finite sequence  $\mathbf{y}$  has a representing measure? If such a measure exists, how do we find it?

[Bayer and Teichmann \[2006\]](#) proved a key result: “if a finite sequence  $\mathbf{y} = (y_\alpha)_{|\alpha| \leq q}$  has a representing measure  $\mu$ , then it has another representing measure  $\nu$  which has finite support with  $\text{supp}(\nu) \subseteq \text{supp}(\mu)$ ”. For truncated moment problems, the question of existence and the subsequent recovery of these finite representing measures require the notion of a *moment matrix* and its associated *flat extension*, see [Laurent \[2009\]](#), [Lasserre \[2010\]](#), [Schmüdgen \[2017\]](#). Towards this end, we denote by  $\mathcal{P}_q(\Omega)$  the space of all polynomials of total degree  $q$ , i.e.,  $\mathcal{P}_q(\Omega) := \text{span}\{\mathbf{x}^\alpha : \mathbf{x} \in \Omega, |\alpha| \leq q\}$ , whose dimension is known to be

$$(2.2) \quad m_q := \binom{q+d}{d}.$$

Letting the row vector

$$(2.3) \quad \boldsymbol{\tau}_q(\mathbf{x}) := \left[ 1, x_1, \dots, x_d, x_1^2, x_1x_2, \dots, x_d^2, \dots, x_1^q, \dots, x_d^q \right]$$

denote the monomial basis in  $\mathcal{P}_q(\Omega)$ , we may express every  $p \in \mathcal{P}_q(\Omega)$  according to

$$p(\mathbf{x}) = \tau_q(\mathbf{x})\mathbf{p} := \sum_{|\alpha| \leq q} p_\alpha \mathbf{x}^\alpha$$

for a suitable coefficient vector  $\mathbf{p} = (p_\alpha)_{|\alpha| \leq q} \in \mathbb{R}^{m_q}$ . Every TMS  $\mathbf{y}$  defines a linear functional  $\mathcal{L}_\mathbf{y}$  acting on  $\mathcal{P}_q(\Omega)$  as

$$\mathcal{L}_\mathbf{y} \left( \sum_{|\alpha| \leq q} p_\alpha \mathbf{x}^\alpha \right) := \sum_{|\alpha| \leq q} p_\alpha y_\alpha.$$

**Definition 2.1.** Let  $\mathbf{y} \in \mathbb{R}^{m_{2q}}$ , cp.(2.1). The moment matrix of order  $q$  is defined as

$$(2.4) \quad \mathbf{M}_\mathbf{y} := \mathcal{L}_\mathbf{y}(\tau_q^\top \tau_q) = [y_{\alpha+\beta}]_{|\alpha|, |\beta| \leq q} \in \mathbb{R}^{m_q \times m_q},$$

where the action of  $\mathcal{L}_\mathbf{y}$  on  $\tau_q^\top \tau_q$  has to be understood element-wise, cp. (2.3). If there exists a vector  $\tilde{\mathbf{y}} \in \mathbb{R}^{m_{2(q+1)}}$  such that  $\tilde{y}_i = y_i$  for  $i = 1, \dots, m_{2q}$  and  $\mathbf{M}_{\tilde{\mathbf{y}}}$  is positive semi-definite with  $\text{rank } \mathbf{M}_{\tilde{\mathbf{y}}} = \text{rank } \mathbf{M}_\mathbf{y}$ , we call  $\mathbf{M}_{\tilde{\mathbf{y}}}$  a flat extension of  $\mathbf{M}_\mathbf{y}$ .

An  $r$ -atomic measure  $\mu$  is a positive linear combination of  $r$  Dirac measures i.e.,

$$(2.5) \quad \mu = \sum_{j=1}^r \lambda_j \delta_{\xi_j}, \quad \lambda_1, \dots, \lambda_r > 0.$$

The points  $\xi_j \in \mathbb{R}^d$  are called the *atoms* of  $\mu$ , which we refer to as *scenarios* in our context. We state the following important result due to [Curto and Fialkow \[1996\]](#) that characterizes TMS having finite representing measures, cp.[Lasserre \[2010\]](#).

**Theorem 2.2** ([\[Curto and Fialkow, 1996\]](#)). Let  $\mathbf{y} \in \mathbb{R}^{m_{2q}}$  with  $\text{rank } \mathbf{M}_\mathbf{y} = r$ . Then  $\mathbf{y}$  has a unique  $r$ -atomic representing measure on  $\mathbb{R}^d$  iff the moment matrix  $\mathbf{M}_\mathbf{y}$  is positive semi-definite and has a flat extension.

A particular consequence of [Theorem 2.2](#) is that any moment matrix  $\mathbf{M}_\mathbf{y} \in \mathbb{R}^{m_q \times m_q}$  associated to an  $r$ -atomic measure  $\mu$  can be represented in the *Vandermonde form*.

$$(2.6) \quad \mathbf{M}_\mathbf{y} = \sum_{j=1}^r \lambda_j \tau_q^\top(\xi_j) \tau_q(\xi_j) = \mathbf{V}_q^\top(\xi_1, \dots, \xi_r) \mathbf{\Lambda} \mathbf{V}_q(\xi_1, \dots, \xi_r),$$

with  $\xi_1, \dots, \xi_r$  the scenarios and their probabilities  $\mathbf{\Lambda} := \text{diag}(\lambda_1, \dots, \lambda_r)$ , see [Lasserre \[2010\]](#), [Schmüdgen \[2017\]](#). In (2.6), the matrix  $\mathbf{V}_q(\xi_1, \dots, \xi_r)$  is the (generalized) Vandermonde matrix

$$(2.7) \quad \mathbf{V}_q(\xi_1, \dots, \xi_r) := \begin{bmatrix} \tau_q(\xi_1) \\ \vdots \\ \tau_q(\xi_r) \end{bmatrix} \in \mathbb{R}^{r \times m_q}.$$

**2.2. Connection to multivariate quadrature.** For a Borel measure  $\mu$  with support  $\Omega \subset \mathbb{R}^d$  and  $\mathcal{P}_q(\Omega) \subset L^1(\Omega, \mu)$ , a quadrature rule of degree  $q$  and size  $m \in \mathbb{N}$  consists of nodes  $\xi_1, \dots, \xi_m$  and positive weights  $\lambda_1, \dots, \lambda_m$  such that

$$(2.8) \quad \int_{\Omega} p(\mathbf{x}) d\mu = \sum_{j=1}^m \lambda_j p(\xi_j) \quad \text{for all } p \in \mathcal{P}_q(\Omega).$$

The next result makes explicit the equivalence between the existence of finite atomic representing measures for TMPs to the existence of quadrature rules in multi-dimensions.

**Theorem 2.3** ([\[Bayer and Teichmann, 2006\]](#)). Let  $\mu$  be a Borel measure with support set  $\Omega \subset \mathbb{R}^d$  such that  $\mathcal{P}_q(\Omega) \subset L^1(\Omega, \mu)$ . Then there exists a quadrature rule of degree  $q$  and size  $1 \leq m \leq m_q$ .

Considering the truncated sequence that is given by the moments of  $\mu$  up to degree  $q$ , the existence of a quadrature rule of degree  $q$ , cp. [Theorem 2.3](#), implies an affirmative answer to the question of having another finite atomic representing measure for the same sequence. The latter measure is given by a linear combination of the Dirac measures supported at the scenarios.

**Remark 2.4.** For a quadrature rule of degree  $q$ , the size estimate  $m_q$  in Theorem 2.3 is not sharp in general. For certain sets and measures, there exist Gaussian-type quadrature rules for which the size is considerably smaller than the one given by Theorem 2.3, see Xu [1994], Fialkow [1999], Curto and Fialkow [2002] and the references therein. Especially in the case  $d = 1$ , any Borel measure on  $\mathbb{R}$  having moments up to degree  $q$  admits a Gaussian quadrature of degree  $q$  with size  $\leq \lfloor q/2 \rfloor + 1$ .

Given a TMS, Lasserre’s algorithm, see [Lasserre, 2010, Algorithm 4.2] relies on the Vandermonde form cp. (2.6) and Theorem 2.2. As a result, this method necessitates computing a flat extension of the moment matrix. However, obtaining a flat extension is difficult, particularly in high dimensions and for  $q > 1$ , see Helton and Nie [2012].

**2.3. Covariance scenarios.** In this paragraph, we suggest an approach for the particular case when  $\mathbf{M}_y \in \mathbb{R}^{m_1 \times m_1}$ ,  $\mathbf{y} \in \mathbb{R}^{m_2}$ . To compute the Vandermonde form as in (2.6) without the need to obtain a flat extension, we rely on Householder reflections, see Householder [1965], for the following theorem.

**Theorem 2.5.** Let  $\mathbf{R} \in \mathbb{R}^{m_1 \times r}$  be a matrix root of the covariance matrix  $\mathbf{M}_y \in \mathbb{R}^{m_1 \times m_1}$ , that is  $\mathbf{M}_y = \mathbf{R}\mathbf{R}^\top$ . Then, the Vandermonde form of  $\mathbf{M}_y$  reads  $\mathbf{M}_y = \mathbf{V}^\top \mathbf{\Lambda} \mathbf{V}$  with  $\mathbf{V} = \sqrt{r} \mathbf{H}_v \mathbf{R}^\top$  and  $\mathbf{\Lambda} = \frac{1}{r} \mathbf{I}$ , where  $\mathbf{H}_v := \mathbf{I} - 2 \frac{\mathbf{v}\mathbf{v}^\top}{\mathbf{v}^\top \mathbf{v}}$  for  $\mathbf{v} := \mathbf{r} - \frac{1}{\sqrt{r}} \mathbf{1}$ . Herein,  $\mathbf{r}^\top$  is the first row of  $\mathbf{R}$  and  $\mathbf{1} \in \mathbb{R}^r$  is the vector of all 1’s.

*Proof.* There holds  $\mathbf{H}_v \mathbf{w} = \mathbf{w}$  for  $\mathbf{w} \perp \mathbf{v}$  and  $\mathbf{H}_v \mathbf{v} = -\mathbf{v}$ . Hence, choosing  $\mathbf{v} = \mathbf{r} - \lambda \mathbf{1}$ , and  $\lambda := \|\mathbf{r}\|_2 / \|\mathbf{1}\|_2 = \|\mathbf{r}\|_2 / \sqrt{r}$ , one readily verifies  $\mathbf{H}_v \mathbf{r} = \lambda \mathbf{1}$ .

Moreover, it is straightforward to see that  $\mathbf{H}_v$  is orthogonal. Therefore, we arrive at the Vandermonde form  $\mathbf{M}_y = \mathbf{R} \mathbf{H}_v^\top \mathbf{H}_v \mathbf{R}^\top = \mathbf{V}^\top \mathbf{\Lambda} \mathbf{V}$  with  $\mathbf{\Lambda} = \lambda^2 \mathbf{I} = \|\mathbf{r}\|_2^2 / r \mathbf{I}$ . Finally, we obtain the assertion by noticing that  $\|\mathbf{r}\|_2^2 = \mathbf{r}^\top \mathbf{r} = (\mathbf{M}_y)_{1,1} = 1$ .  $\square$

Theorem 2.5 demonstrates that it is possible to match up to second moments exactly using unique scenarios from any input moment matrix of degree one. The reason this yields unique scenarios without a flat extension of the moment matrix lies in the uniform distribution of the weights. The restriction to  $q = 1$  is due to preserving the Vandermonde form, which could otherwise not be guaranteed. We list the computational steps of Theorem 2.5 in Algorithm 2.1. We refer to the unique scenarios obtained from this algorithm as *covariance scenarios*. It yields a new decomposition of moment matrices up to second order in terms of scenarios  $\xi_1, \dots, \xi_r$  computed according to 2.1 below, each realizing with probability  $1/r$ .

---

**Algorithm 2.1** Covariance scenarios

---

**input:** symmetric and positive semidefinite moment matrix  $\mathbf{M}_y \in \mathbb{R}^{m_1 \times m_1}$ , tolerance  $\varepsilon > 0$

**output:** scenarios  $\Xi := \{\xi_1, \dots, \xi_r\} \subset \mathbb{R}^d$

- 1: compute a matrix root  $\mathbf{M}_y = \mathbf{R}\mathbf{R}^\top$
  - 2: set  $\mathbf{r} := \mathbf{R}^\top \mathbf{e}_1$ ,  $\lambda := 1/\sqrt{r}$ ,  $\mathbf{v} := \mathbf{r} - \lambda \mathbf{1}$ ,  $\gamma := 2/\|\mathbf{v}\|_2^2$
  - 3: set  $\mathbf{H}_v := \mathbf{I} - \gamma \mathbf{v}\mathbf{v}^\top$  and  $\mathbf{V} := \frac{1}{\lambda} \mathbf{H}_v \mathbf{R}^\top$
  - 4: set  $\xi_j = [\mathbf{V}^\top \mathbf{e}_j]_{i=2}^{d+1}$  for  $j = 1, \dots, r$
- 

Note that the *covariance scenarios* grant consistent use of moments and scenarios, which is important for certain applications, as noted already in the introduction. In finance, for instance, portfolio optimization usually requires covariance matrices, while risk management is scenario-based. The construction introduced above guarantees that both function in lockstep. Furthermore, the extracted covariance scenarios would typically reflect future potential instances of the cross-section of asset returns and can be used for generative modeling of the risk landscape of the assets.

### 3. THE EMPIRICAL MOMENT PROBLEM

In this section, we consider the case when the underlying probability measure is known empirically from i.i.d. draws, as is typically assumed in data-driven applications. We first formulate the problem as an

empirical alternative to the truncated moment problem of Section 2. We then propose a reformulation of the problem in an appropriate RKHS that can be used to embed the polynomial moments of the samples.

**3.1. Problem formulation.** Let  $X = \{\mathbf{x}_1, \dots, \mathbf{x}_N\} \subset \Omega \subset \mathbb{R}^d$ , denote the set of data samples. The associated empirical measure is given by

$$\widehat{\mathbb{P}} := \frac{1}{N} \sum_{i=1}^N \delta_{\mathbf{x}_i}.$$

It satisfies  $\widehat{\mathbb{P}}(X) = 1$ , and is hence a probability measure. With the empirical measure at hand, it is straightforward to compute the associated empirical truncated moment sequence

$$(3.1) \quad \widehat{\mathbf{y}} = [\widehat{y}_{\alpha}]_{|\alpha| \leq 2q} = \left[ \int_{\Omega} \mathbf{x}^{\alpha} d\widehat{\mathbb{P}} \right]_{|\alpha| \leq 2q} = \frac{1}{N} \sum_{i=1}^N \boldsymbol{\tau}_{2q}^{\top}(\mathbf{x}_i) = \frac{1}{N} \mathbf{V}_{2q}^{\top}(\mathbf{x}_1, \dots, \mathbf{x}_N) \mathbf{1} \in \mathbb{R}^{m_{2q}}.$$

With  $\widehat{\mathbf{y}}$  admitting  $\widehat{\mathbb{P}}$  as a representing measure, we focus on performing moment-matching with respect to the empirical measure for accurate scenario-based representation of the data samples. In analogy to Section 2, we thus pose the EMP: Does the empirical TMS  $\widehat{\mathbf{y}}$  admit another representing probability measure  $\mathbb{P}^*$  such that  $\text{supp}(\mathbb{P}^*) \subset \text{supp}(\widehat{\mathbb{P}})$ ? If such a measure exists, then how to obtain it?

Note that under the assumption of  $\text{supp}(\mathbb{P}^*) \subset \text{supp}(\widehat{\mathbb{P}})$ , we seek an appropriate set of scenarios  $\Xi := \{\boldsymbol{\xi}_1, \dots, \boldsymbol{\xi}_m\} \subset X$  with  $m \ll N$ . This corresponds to a compressed version of the sample measure, i.e.,

$$(3.2) \quad \mathbb{P}^* = \sum_{j=1}^m \lambda_j \delta_{\boldsymbol{\xi}_j}, \quad \lambda_j \geq 0, \quad \sum_{j=1}^m \lambda_j = 1,$$

with the associated truncated moment sequence

$$(3.3) \quad \mathbf{y}^* = [y_{\alpha}^*]_{|\alpha| \leq 2q} = \left[ \int_{\Omega} \mathbf{x}^{\alpha} d\mathbb{P}^* \right]_{|\alpha| \leq 2q} = \mathbf{V}_{2q}^{\top}(\boldsymbol{\xi}_1, \dots, \boldsymbol{\xi}_m) \boldsymbol{\Lambda}, \quad \boldsymbol{\Lambda} := [\lambda_1, \dots, \lambda_m]^{\top}.$$

As mentioned in Remark 2.4, for  $d = 1$ , Gaussian quadrature rules are efficient for the moment-matching problem since they use the optimal number of scenarios that match moments for the highest polynomial degree. In multiple dimensions, however, generalizing Gaussian quadrature is computationally challenging, and thus retrieving the optimal number of scenarios for the EMP is rather challenging. In particular, with regard to any representing measure  $\mu$  for a truncated sequence  $\mathbf{y}$ , we have, in general, that  $|\text{supp}(\mu)| \geq \text{rank}(\mathbf{M}_{\mathbf{y}})$ , see [Curto and Fialkow \[1996\]](#), [Fialkow \[1999\]](#).

To obtain scenarios that accurately reflect the data while remaining computationally efficient, we consider a relaxed version of the EMP and determine the vector  $\mathbf{y}^*$  such that

$$(3.4) \quad \|\mathbf{y}^* - \widehat{\mathbf{y}}\| \leq \varepsilon$$

for a given tolerance  $\varepsilon > 0$  and a given norm  $\|\cdot\|$  on  $\mathbb{R}^{m_{2q}}$ .

Note that with the assumption of the scenarios as a subset of the samples, we can write  $\mathbf{y}^* = \mathbf{V}_{2q}^{\top}(\mathbf{x}_1, \dots, \mathbf{x}_N) \mathbf{w}$  where  $\mathbf{w} \in \mathbb{R}^N$  has at most  $m$  non-zero entries. Thus, constructing  $\mathbf{y}^*$  in (3.4) is equivalent to a particular strategy of column subsampling of  $\mathbf{V}_{2q}^{\top}(\mathbf{x}_1, \dots, \mathbf{x}_N)$ . This can be performed by ensuring only certain entries of  $\mathbf{w}$  are non-zero. However, this is not enough to ensure the convexity of the weights. With this in mind, to simultaneously ensure that the weights are normalized and positive, we solve the problem in two stages. First, setting the norm in (3.4) to be the Euclidean norm,  $\|\cdot\|_2$ , we extract the scenarios following a greedy paradigm that constructs a *sparse weight vector*  $\mathbf{w} \in \mathbb{R}^N$  such that

$$(3.5) \quad \|\mathbf{V}_{2q}^{\top}(\mathbf{x}_1, \dots, \mathbf{x}_N) \mathbf{w} - \widehat{\mathbf{y}}\|_2 \leq \varepsilon.$$

Note that the Euclidean norm corresponds to the mean squared error in the approximation. Alternatively, one can set the sup-norm for the worst-case error. Second, we retrieve the corresponding probabilities by enforcing the simplex constraints  $\Delta := \{\mathbf{w} : \mathbf{w} \geq \mathbf{0}, \mathbf{1}^{\top} \mathbf{w} = 1\}$  with a standard algorithm in Section 4.2.

For now, we focus on Problem 3.5 for the extraction of good representative scenarios. Although (3.5) is trivially minimized at the constant vector with element  $1/N$ , nevertheless, it is underdetermined in the regime  $m_{2q} \ll N$  when we have a large number of samples. Hence, we need a computational framework

that helps us in choosing a good representative subspace of  $\text{Im}(\mathbf{V}_{2q}^\top(\mathbf{x}_1, \dots, \mathbf{x}_N))$ . Towards that end, we propose to use an RKHS framework that allows us to do the above.

**3.2. Reformulation in RKHS.** Our main reason for the reformulation in an RKHS setting is as follows: with our assumption that the finite atomic target measure  $\mathbb{P}^* \ll \widehat{\mathbb{P}}$ , we are essentially looking to extract the optimal support set for  $\mathbb{P}^*$  when solving Problem 3.5. We want  $\mathbb{P}^*$  and  $\widehat{\mathbb{P}}$  to be pointwise close. One key property of an RKHS is that, if two functions are close in the RKHS norm, then they are pointwise close as well. This works to our advantage since we want to express the empirical polynomial moments using fewer scenarios.

For completeness, we provide the definition of the RKHS below, see Paulsen and Raghupathi [2016], Berlinet and Thomas-Agnan [2011], for further details.

**Definition 3.1.** Let  $(\mathcal{H}, \langle \cdot, \cdot \rangle_{\mathcal{H}})$  be a Hilbert space of real-valued functions on a non-empty set  $\Omega$ . A function  $\mathcal{K}: \Omega \times \Omega \rightarrow \mathbb{R}$  is a reproducing kernel of the Hilbert space  $\mathcal{H}$  iff

$$(3.6) \quad \begin{aligned} \mathcal{K}(\mathbf{x}, \cdot) &\in \mathcal{H} \quad \text{for all } \mathbf{x} \in \Omega \\ \langle \mathcal{K}(\mathbf{x}, \cdot), h \rangle_{\mathcal{H}} &= h(\mathbf{x}) \quad \text{for all } \mathbf{x} \in \Omega, h \in \mathcal{H}. \end{aligned}$$

The last condition of Equation (3.6) is called the reproducing property. If these two properties hold, then  $(\mathcal{H}, \langle \cdot, \cdot \rangle_{\mathcal{H}})$  is called a reproducing kernel Hilbert space.

In practice, given a finite set of data samples  $X := \{\mathbf{x}_1, \dots, \mathbf{x}_N\} \subset \Omega \subset \mathbb{R}^d$ , we work in the subspace of kernel translates  $\mathcal{H}_X := \text{span}\{\mathcal{K}(\mathbf{x}_i, \cdot) : \mathbf{x}_i \in X\}$ .

We wish to embed the polynomial moments of the samples in the RKHS such that it is spanned by the columns of  $\mathbf{V}_{2q}^\top(\mathbf{x}_1, \dots, \mathbf{x}_N)$ . Hence, we consider  $\mathcal{P}_{2q}(X)$  endowed with the  $L_{\widehat{\mathbb{P}}}^2$ -inner product. We can set the basis of  $\mathcal{H}_X$  to be the standard basis  $\mathbf{U}(\mathbf{x}) := \boldsymbol{\tau}_{2q}^\top(\mathbf{x})$ , where each column vector is now treated as a function in  $\mathcal{H}_X$ . We also define  $\mathbf{U} := [\mathbf{U}(\mathbf{x}_1), \dots, \mathbf{U}(\mathbf{x}_N)]$  to be the basis functions evaluated at the samples, which is just  $\mathbf{V}^\top$ . However, the standard bases of kernel translates are known to have poor conditioning, see De Marchi and Schaback [2010]. Furthermore, in most practical applications involving large data samples, we typically have  $m_{2q} \ll N$ . Therefore, we seek a suitable *data-dependent* basis for  $\mathcal{H}_X$  such that it is amenable to the task at hand. For this, we introduce an appropriate representation of the reproducing kernel. Toward that end, we first compute the Gram matrix as follows,

$$\langle \mathbf{U}, \mathbf{U}^\top \rangle_{\mathcal{H}_X} = \langle \boldsymbol{\tau}_{2q}^\top, \boldsymbol{\tau}_{2q} \rangle_{L_{\widehat{\mathbb{P}}}^2(X)} = \left[ \int_X \mathbf{x}^{\alpha+\beta} d\widehat{\mathbb{P}} \right]_{|\alpha|, |\beta| \leq 2q} = \frac{1}{N} \mathbf{V}_{2q}^\top(\mathbf{x}_1, \dots, \mathbf{x}_N) \mathbf{V}_{2q}(\mathbf{x}_1, \dots, \mathbf{x}_N),$$

which turns out to be the empirical moment matrix of order  $2q$ , which we will write henceforth as  $\mathbf{M}$ . There holds for the reproducing kernel restricted to  $\mathcal{H}_X$  that

$$(3.7) \quad \mathcal{K}(\mathbf{x}, \mathbf{x}') = \mathbf{U}(\mathbf{x})^\top \mathbf{M}^\dagger \mathbf{U}(\mathbf{x}').$$

Herein,  $\mathbf{M}^\dagger$  denotes the Moore-Penrose inverse of  $\mathbf{M}$ . Associated with the kernel  $\mathcal{K}$ , we introduce the canonical feature map  $\Phi: X \rightarrow \mathcal{H}_X, \Phi(\mathbf{x}) \mapsto \mathcal{K}(\mathbf{x}, \cdot)$  that embeds the data from  $X$  into the Hilbert space of functions. We denote the basis of kernel translates by

$$(3.8) \quad \Phi(\mathbf{x}) := [\mathcal{K}(\mathbf{x}, \mathbf{x}_1), \dots, \mathcal{K}(\mathbf{x}, \mathbf{x}_N)].$$

For the sake of completeness, we show that the kernel defined in (3.7) is indeed the *reproducing kernel* on  $\mathcal{H}_X$ .

**Theorem 3.2.** The function  $\mathcal{K}: X \times X \rightarrow \mathbb{R}$  as defined in (3.7) is a symmetric and positive type function. Moreover,  $\mathcal{K}$  has the reproducing property on  $X$ ,

$$(3.9) \quad \langle \mathcal{K}(\mathbf{x}_i, \cdot), p \rangle_{\mathcal{H}_X} = p(\mathbf{x}_i) \quad \text{for all } \mathbf{x}_i \in X, p \in \mathcal{H}_X.$$

*Proof.* For the sake of a lighter notation, we will henceforth write  $\mathbf{V} := \mathbf{V}_{2q}(\mathbf{x}_1, \dots, \mathbf{x}_N) \in \mathbb{R}^{N \times m_{2q}}$ . We introduce the kernel matrix

$$(3.10) \quad \mathbf{K} := [\mathcal{K}(\mathbf{x}_i, \mathbf{x}_j)]_{i,j=1}^N = \mathbf{U}^\top \mathbf{M}^\dagger \mathbf{U} = \mathbf{V} \mathbf{M}^\dagger \mathbf{V}^\top \in \mathbb{R}^{N \times N}.$$

The matrix  $\mathbf{K}$  is symmetric, which follows from the fact that  $\mathbf{M}^\dagger$  is symmetric. There holds  $\mathbf{M}^\dagger = \mathbf{N}\mathbf{V}^\dagger(\mathbf{V}^\top)^\dagger$ . Note that  $\text{rank } \mathbf{K} = \text{rank } \mathbf{M}$ . Furthermore, we have

$$\mathbf{a}^\top \mathbf{K} \mathbf{a} = \mathbf{N} \mathbf{a}^\top \mathbf{V} \mathbf{V}^\dagger (\mathbf{V}^\top)^\dagger \mathbf{V}^\top \mathbf{a} = N \|(\mathbf{V}^\top)^\dagger \mathbf{V}^\top \mathbf{a}\|_2^2 \geq 0 \quad \text{for all } \mathbf{a} \in \mathbb{R}^N$$

Hence, the matrix  $\mathbf{K}$  is symmetric and positive semi-definite, i.e., the kernel  $\mathcal{K}$  is a symmetric and positive type function. In order to prove the reproducing property, we first recall that the Moore-Penrose inverse satisfies  $\mathbf{A}\mathbf{A}^\dagger\mathbf{A} = \mathbf{A}$ ,  $(\mathbf{A}\mathbf{A}^\top)^\dagger = (\mathbf{A}^\top)^\dagger\mathbf{A}^\dagger$  as well as  $(\mathbf{A}\mathbf{A}^\dagger)^\top = \mathbf{A}\mathbf{A}^\dagger$  for any matrix  $\mathbf{A}$ . From this, we directly infer

$$(3.11) \quad \mathbf{V}(\mathbf{M}^\dagger\mathbf{M}) = \mathbf{V}\left((\mathbf{V}^\top\mathbf{V})^\dagger\mathbf{V}^\top\mathbf{V}\right) = \left((\mathbf{V}\mathbf{V}^\dagger)(\mathbf{V}\mathbf{V}^\dagger)^\top\right)\mathbf{V} = (\mathbf{V}\mathbf{V}^\dagger)(\mathbf{V}\mathbf{V}^\dagger)\mathbf{V} = \mathbf{V}.$$

Let  $p \in \mathcal{H}_X \equiv \mathcal{P}_{2q}(X)$ , i.e.,  $p(\mathbf{x}_i) = \boldsymbol{\tau}_{2q}(\mathbf{x}_i)\mathbf{p}$  for any coefficient vector  $\mathbf{p} \in \mathbb{R}^{m_{2q}}$  and any  $\mathbf{x}_i \in X$ . Hence,

$$\langle \mathcal{K}(\mathbf{x}_i, \cdot), p \rangle_{\mathcal{H}_X} = \boldsymbol{\tau}_{2q}(\mathbf{x}_i) \mathbf{M}^\dagger \langle \boldsymbol{\tau}_{2q}^\top, \boldsymbol{\tau}_{2q} \rangle_{L_{\mathbb{P}}^2(X)} \mathbf{p} = \boldsymbol{\tau}_{2q}(\mathbf{x}_i) \mathbf{M}^\dagger \mathbf{M} \mathbf{p} = \boldsymbol{\tau}_{2q}(\mathbf{x}_i) \mathbf{p} = p(\mathbf{x}_i),$$

where we use (3.11) and that  $[\mathbf{V}_{i,j}]_{j=1}^{m_{2q}} = \boldsymbol{\tau}_{2q}(\mathbf{x}_i)$ .  $\square$

**Corollary 3.3.** *A consequence of the reproducing property is  $\mathbf{K}\mathbf{V} = \mathbf{N}\mathbf{V}$ .*

We close this paragraph by providing an algorithm for the computation of an orthonormal basis for  $\mathcal{H}_X$ . Any general data-dependent basis turns out to be defined via a factorization of the Gram matrix defined by these data, see Pazouki and Schaback [2011]. Various matrix factorizations give rise to different bases with different properties. For our purpose, we apply the pivoted Cholesky factorization, see Harbrecht et al. [2012], as in Algorithm 3.1 on the positive semi-definite moment matrix  $\mathbf{M}$ . With a sufficiently low error tolerance  $\varepsilon$ , we obtain  $m_{2q} \times r$  matrices  $\mathbf{B}_M$  and  $\mathbf{L}_M$  with  $r = \text{rank}(\mathbf{M}) \leq m_{2q}$  such that

$$\text{tr}(\mathbf{M} - \mathbf{L}_M \mathbf{L}_M^\top) \leq \varepsilon, \quad \mathbf{B}_M^\top \mathbf{L}_M = \mathbf{I}_r, \quad \mathbf{M} \mathbf{B}_M = \mathbf{L}_M.$$

We particularly have  $\mathbf{M}^\dagger = \mathbf{B}_M \mathbf{B}_M^\top$ . The basis transformation is an essential byproduct of efficiently solving the low-rank approximation of the unconstrained optimization problem at a large scale.

---

**Algorithm 3.1** Pivoted Cholesky Decomposition (Harbrecht et al. [2012])

---

**input:** symmetric and positive semi-definite matrix  $\mathbf{M} \in \mathbb{R}^{m_{2q} \times m_{2q}}$ ,  
tolerance  $\varepsilon \geq 0$

**output:** low-rank approximation  $\mathbf{M} \approx \mathbf{L}_M \mathbf{L}_M^\top$   
and biorthogonal basis  $\mathbf{B}_M$  such that  $\mathbf{B}_M^\top \mathbf{L}_M = \mathbf{I}_r$

- 1: Initialization: set  $r := 1$ ,  $\mathbf{d} := \text{diag}(\mathbf{M})$ ,  $\mathbf{L}_M := []$ ,  $\mathbf{B}_M := []$ ,  $\text{err} := \|\mathbf{d}\|_1$
- 2: **while**  $\text{err} > \varepsilon$
- 3:     determine  $\pi(r) := \arg \max_{1 \leq i \leq m_{2q}} d_i$
- 4:     compute

$$\boldsymbol{\ell}_r := \frac{1}{\sqrt{d_{\pi(r)}}} \left( \mathbf{M} - \mathbf{L}_M \mathbf{L}_M^\top \right) \mathbf{e}_{\pi(r)} \quad \text{and} \quad \mathbf{b}_r := \frac{1}{\sqrt{d_{\pi(r)}}} \left( \mathbf{I} - \mathbf{B}_M \mathbf{L}_M^\top \right) \mathbf{e}_{\pi(r)}$$

- 5:     set  $\mathbf{L}_M := [\mathbf{L}_M, \boldsymbol{\ell}_r]$ ,  $\mathbf{B}_M := [\mathbf{B}_M, \mathbf{b}_r]$
  - 6:     set  $\mathbf{d} := \mathbf{d} - \boldsymbol{\ell}_r \odot \boldsymbol{\ell}_r$ , where  $\odot$  denotes the Hadamard product
  - 7:     set  $\text{err} := \|\mathbf{d}\|_1$ ,  $r := r + 1$
- 

Using the bi-orthogonal basis  $\mathbf{B}_M$  arising out of the pivoted Cholesky algorithm, we define the matrix

$$(3.12) \quad \mathbf{Q} := \frac{1}{\sqrt{N}} \mathbf{V} \mathbf{B}_M \in \mathbb{R}^{N \times r}$$

that satisfies  $\mathbf{Q}^\top \mathbf{Q} = \mathbf{I}_r$ . The matrix  $\mathbf{K}$  can be decomposed as

$$(3.13) \quad \mathbf{K} = \mathbf{N} \mathbf{Q} \mathbf{Q}^\top.$$

The above decomposition shows that the kernel matrix is simply the projection onto the columns spanned by the isometry and in particular, we have  $\text{Im}(\mathbf{V}) = \text{Im}(\mathbf{Q}) = \text{Im}(\mathbf{K})$ . With the above insights, we prove the following result, which will help in the numerical solution of problem (3.5).



**Theorem 3.4.** *Defining  $\tilde{\mathbf{y}} := \frac{1}{\sqrt{N}} \mathbf{B}_M^\top \hat{\mathbf{y}}$ , we have the following conditioning relation,*

$$\frac{\sigma_{\min}(\mathbf{M}^\dagger)}{N} \cdot \|\mathbf{V}^\top \mathbf{w} - \hat{\mathbf{y}}\|_2^2 \leq \|\mathbf{Q}^\top \mathbf{w} - \tilde{\mathbf{y}}\|_2^2 \leq \frac{\sigma_{\max}(\mathbf{M}^\dagger)}{N} \cdot \|\mathbf{V}^\top \mathbf{w} - \hat{\mathbf{y}}\|_2^2.$$

*Proof.* For the right-side inequality, we have

$$\|\mathbf{Q}^\top \mathbf{w} - \tilde{\mathbf{y}}\|_2^2 = \left\| \frac{1}{\sqrt{N}} \mathbf{B}_M^\top (\mathbf{V}^\top \mathbf{w} - \hat{\mathbf{y}}) \right\|_2^2 \leq \frac{1}{N} \|\mathbf{B}_M^\top\|_2^2 \cdot \|\mathbf{V}^\top \mathbf{w} - \hat{\mathbf{y}}\|_2^2$$

and noticing that  $\|\mathbf{B}_M^\top\|_2^2 = \sigma_{\max}(\mathbf{B}_M \mathbf{B}_M^\top) = \sigma_{\max}(\mathbf{M}^\dagger)$ . For the left-side inequality, we have

$$\begin{aligned} \|\mathbf{V}^\top \mathbf{w} - \hat{\mathbf{y}}\|_2^2 &= \left\| \mathbf{V}^\top \left( \mathbf{w} - \frac{1}{N} \mathbf{1} \right) \right\|_2^2 = \left\| \frac{1}{N} \mathbf{V}^\top \mathbf{K} \left( \mathbf{w} - \frac{1}{N} \mathbf{1} \right) \right\|_2^2 = \left\| \mathbf{V}^\top \mathbf{Q} \mathbf{Q}^\top \left( \mathbf{w} - \frac{1}{N} \mathbf{1} \right) \right\|_2^2 \\ &= \|\mathbf{V}^\top \mathbf{Q} \mathbf{Q}^\top \mathbf{w} - \mathbf{V}^\top \mathbf{Q} \tilde{\mathbf{y}}\|_2^2 \leq \|\mathbf{V}^\top\|_2^2 \cdot \|\mathbf{Q}(\mathbf{Q}^\top \mathbf{w} - \tilde{\mathbf{y}})\|_2^2 = \|\mathbf{V}^\top\|_2^2 \cdot \|\mathbf{Q}^\top \mathbf{w} - \tilde{\mathbf{y}}\|_2^2 \end{aligned}$$

where the second equality on the first line follows from (3.3), and the last equality is due to  $\mathbf{Q}$  being an isometry. Thus, using the decomposition of the moment matrix  $\mathbf{M} = (\mathbf{V}^\top \mathbf{V})/N$ , we have that  $\|\mathbf{V}^\top\|_2^2 = N\sigma_{\max}(\mathbf{M}) = N/\sigma_{\min}(\mathbf{M}^\dagger)$ .  $\square$

**Remark 3.5.** *The normal equations of Problem 3.5 reads  $\mathbf{V} \mathbf{V}^\top \mathbf{w} = \mathbf{V} \hat{\mathbf{y}}$ , so that the condition number of the system is  $\kappa(\mathbf{V} \mathbf{V}^\top) = \kappa(\mathbf{V}^\top \mathbf{V}) = \kappa(\mathbf{M})$ . Now, the condition number of Problem 3.14 is  $\kappa(\mathbf{Q} \mathbf{Q}^\top) = \kappa(\mathbf{Q}^\top \mathbf{Q}) = 1$ . Hence, the above proposition shows that, up to  $\kappa(\mathbf{M})$ , (3.5) is equivalent to*

$$(3.14) \quad \|\mathbf{Q}^\top \mathbf{w} - \tilde{\mathbf{y}}\|_2,$$

*which we will henceforth consider for the greedy extraction of scenarios, instead of (3.5).*

In the next result, we collect additional properties of  $\mathbf{Q}$ , in particular in connection with the above optimization problem.

**Lemma 3.6.** *Matrix  $\mathbf{Q}$  satisfies the relation*

$$(3.15) \quad \mathbf{Q} \tilde{\mathbf{y}} = \frac{1}{N} \mathbf{1}.$$

*From the normal equations  $\mathbf{Q} \mathbf{Q}^\top \mathbf{w} = \mathbf{Q} \tilde{\mathbf{y}}$ , vector  $\mathbf{w} = \frac{1}{N} \mathbf{1}$  is a solution of (3.14).*

*Proof.* To show (3.15), we first note that  $\hat{\mathbf{y}}$  can be identified with the first column of the moment matrix, i.e.,  $\hat{\mathbf{y}} = \mathbf{M} \mathbf{e}_1 = \frac{1}{N} \mathbf{V}^\top \mathbf{V} \mathbf{e}_1$ . Hence, we can write

$$(3.16) \quad \mathbf{Q} \tilde{\mathbf{y}} = \frac{1}{N} \mathbf{V} \mathbf{B}_M \mathbf{B}_M^\top \mathbf{M} \mathbf{e}_1 = \frac{1}{N} \mathbf{V} \mathbf{M}^\dagger \mathbf{M} \mathbf{e}_1 = \frac{1}{N} \mathbf{V} \mathbf{e}_1 = \frac{1}{N} \mathbf{1},$$

where we exploit the reproducing property of the kernel on the sample set, cp. (3.11), and the identity  $\mathbf{M}^\dagger = \mathbf{B}_M \mathbf{B}_M^\top$ . We have as a corollary

$$\mathbf{Q} \tilde{\mathbf{y}} = \frac{1}{N} \mathbf{1} = \mathbf{Q} \mathbf{Q}^\top \frac{1}{N} \mathbf{1},$$

again by (3.11) and the fact that  $\mathbf{V} \mathbf{e}_1 = \mathbf{1}$ . Hence, the vector  $\mathbf{w} = \frac{1}{N} \mathbf{1}$  is a solution to the normal equations.  $\square$

#### 4. ALGORITHMS FOR SCENARIO REPRESENTATION

In this section, we present the algorithms for the two stages as mentioned in Section 3. The first algorithm, *orthogonal matching pursuit* (OMP), see [Pazouki and Schaback \[2011\]](#), is devised to extract the scenarios in a greedy manner. The second is the *alternating direction method of multipliers* (ADMM), see [Boyd \[2011\]](#), and is used for retrieving the corresponding probabilities.

**4.1. Step 1: Scenario extraction.** For the scenario extraction problem, we first note that a minimum-norm solution of Problem 3.14 satisfies the normal equations

$$(4.1) \quad \mathbf{Q} \mathbf{Q}^\top \mathbf{w} = \mathbf{Q} \tilde{\mathbf{y}} = \frac{1}{N} \mathbf{1}, \quad \text{which implies} \quad \mathbf{K} \mathbf{w} = \mathbf{1},$$

where the second equality is due to Lemma 3.6. Suppose that  $h \in \mathcal{H}_X$  is a function such that its evaluation on the samples gives the vector of ones i.e.  $[h(\mathbf{x}_i)]_{i=1}^N = \mathbf{1}$ . Any  $\mathbf{w} \in \mathbb{R}^N$  satisfying the equation  $\mathbf{K}\mathbf{w} = \mathbf{1}$  defines an interpolant  $s_h \in \mathcal{H}_X$  which can be written as

$$s_h(\mathbf{x}) = \sum_{i=1}^N w_i \mathcal{K}(\mathbf{x}, \mathbf{x}_i) = \Phi(\mathbf{x})\mathbf{w} \quad \text{for all } \mathbf{x} \in X,$$

where  $\Phi(\mathbf{x})$  is from (3.8). More generally, any interpolant that exactly matches  $m$  entries of  $h$  has the form

$$(4.2) \quad s_{h,m}(\mathbf{x}) := \sum_{j=1}^m w_j \mathcal{K}(\mathbf{x}, \xi_j) \quad \text{for all } \mathbf{x} \in X,$$

where  $\{\xi_1, \dots, \xi_m\} \subset X$ . The interpolant  $s_{h,m} \in \text{span}\{\mathcal{K}(\cdot, \xi_1), \dots, \mathcal{K}(\cdot, \xi_m)\}$  and the problem of choosing a few number of scenarios from a large set of samples is therefore equivalent to choosing a subset from the dictionary  $\{\mathcal{K}(\cdot, \mathbf{x}_1), \dots, \mathcal{K}(\cdot, \mathbf{x}_N)\}$ . Hereby, we resort to a greedy subsampling of the columns of  $\mathbf{K}$  that can approximate its column space within a certain error tolerance. With this objective in mind, we adapt the notion of the pivoted Cholesky decomposition of  $\mathbf{K}$  into the setting of Algorithm 4.1 as below.

---

**Algorithm 4.1** Orthogonal matching pursuit (OMP)

---

**input:** symmetric and positive semi-definite matrix  $\mathbf{K} \in \mathbb{R}^{N \times N}$ ,  
tolerance  $\varepsilon > 0$

**output:** index set  $\pi$  corresponding to the sparse scenarios  $\Xi := \{\xi_1, \dots, \xi_m\} \subset \mathbb{R}^d$ ,  
low-rank approximation  $\mathbf{K} \approx \mathbf{L}_m \mathbf{L}_m^\top$   
and bi-orthogonal basis  $\mathbf{B}_m$  such that  $\mathbf{B}_m^\top \mathbf{L}_m = \mathbf{I}_m$

- 1: Initialization: set  $m := 1$ ,  $\mathbf{L}_0 := []$ ,  $\mathbf{B}_0 := []$ ,  $\pi := []$ ,  $\mathbf{d}_0 = \text{diag}(\mathbf{K})$ ,  $\mathbf{h}_0 = \mathbf{1}$ , err = 1
- 2: **while** err >  $\varepsilon$
- 3:   determine  $\pi(m) := \arg \max_{1 \leq i \leq N} |h_{m-1, i}|$
- 4:    $\pi := [\pi, \pi(m)]$
- 5:   compute

$$\ell_m := \frac{1}{\sqrt{d_{m-1, \pi(m)}}} \left( \mathbf{K} - \mathbf{L}_{m-1} \mathbf{L}_{m-1}^\top \right) \mathbf{e}_{\pi(m)} \quad \text{and} \quad \mathbf{b}_m := \frac{1}{\sqrt{d_{m-1, \pi(m)}}} \left( \mathbf{I} - \mathbf{B}_{m-1} \mathbf{L}_{m-1}^\top \right) \mathbf{e}_{\pi(m)}$$

- 6:   set  $\mathbf{L}_m := [\mathbf{L}_{m-1}, \ell_m]$ ,  $\mathbf{B}_m := [\mathbf{B}_{m-1}, \mathbf{b}_m]$
  - 7:   set  $\mathbf{h}_m := \mathbf{h}_{m-1} - (\mathbf{b}_m^\top \mathbf{h}_0) \ell_m$
  - 8:   set  $\mathbf{d}_m := \mathbf{d}_{m-1} - \ell_m \odot \ell_m$ , where  $\odot$  denotes the Hadamard product
  - 9:   set err :=  $\|\mathbf{h}_m\|_2 / \|\mathbf{h}_0\|_2$ ,  $m := m + 1$
- 

The bi-orthogonal basis  $\mathbf{B}_m$  issuing from the Algorithm 4.1 can be used to define an orthonormal set of basis functions. We define the *Newton basis* as  $\mathbf{N}(\mathbf{x}) := \Phi(\mathbf{x})\mathbf{B}_m$ , see Pazouki and Schaback [2011]. The Newton basis evaluated on the set of samples  $X$  gives

$$(4.3) \quad \mathbf{N} := [N(\mathbf{x}_i)]_{i=1}^N = [\Phi(\mathbf{x}_i)\mathbf{B}_m]_{i=1}^N = \mathbf{K}\mathbf{B}_m = \mathbf{L}_m.$$

Hence, we have that the column vectors of  $\mathbf{L}_m$  of Algorithm 4.1, i.e.,  $\ell_1, \dots, \ell_m$  is just the Newton basis evaluated at the sample points. Denoting the  $m$  basis functions as  $N_1, \dots, N_m$ , we have that

$$\text{Im}(\mathbf{L}_m) = \text{span}\{N_1, \dots, N_m\} = \text{span}\{\mathcal{K}(\cdot, \mathbf{x}_{\pi(1)}), \dots, \mathcal{K}(\cdot, \mathbf{x}_{\pi(m)})\} \subset \text{span}\{\mathcal{K}(\cdot, \mathbf{x}_1), \dots, \mathcal{K}(\cdot, \mathbf{x}_N)\} = \mathcal{H}_X.$$

Furthermore, they form an orthonormal system in  $\mathcal{H}_X$  i.e.  $\langle N_i, N_j \rangle_{\mathcal{H}_X} = \delta_{i,j}$  for  $1 \leq i, j \leq m$ , since

$$\langle \mathbf{N}^\top, \mathbf{N} \rangle_{\mathcal{H}_X} = \mathbf{B}_m^\top \langle \Phi^\top, \Phi \rangle_{\mathcal{H}_X} \mathbf{B}_m = \mathbf{B}_m^\top \mathbf{K} \mathbf{B}_m = \mathbf{B}_m^\top \mathbf{L}_m = \mathbf{I}_m.$$

Therefore, the Newton basis functions  $N_1, \dots, N_m$  are an orthonormal basis for the space of the kernel translates  $\mathcal{K}(\cdot, \mathbf{x}_{\pi(1)}), \dots, \mathcal{K}(\cdot, \mathbf{x}_{\pi(m)})$ . This basis is adaptively constructed by means of a Gram-Schmidt procedure to represent the function  $h \in \mathcal{H}$ , i.e.,

$$h_m = h_{m-1} - N_m \langle N_m, h \rangle_{\mathcal{H}_X} = h - \sum_{j=1}^m N_j \langle N_j, h \rangle_{\mathcal{H}_X} =: h - P_{\mathcal{F}} h.$$

From Algorithm 4.1 line 6, the vector of evaluations of  $h_m$  has the form  $\mathbf{h}_m = (\mathbf{I} - \mathbf{L}_m \mathbf{B}_m^\top) \mathbf{h}_0$ . Therefore, the component of  $h_0$  in the direction of  $N_m$  i.e.,  $N_m \langle N_m, h_0 \rangle_{\mathcal{H}_X}$  has the vector form  $\ell_m(\mathbf{b}_m^\top \mathbf{h}_0)$ . Line 7 of Algorithm 4.1 computes exactly this error between  $h_0$  and its orthogonal projection onto the subspace spanned by  $N_1, \dots, N_m$ . By standard arguments, we have that the mean-squared error satisfies

$$(4.4) \quad \frac{1}{N} \sum_{i=1}^N (h(\mathbf{x}_i) - h_{\mathcal{F}}(\mathbf{x}_i))^2 \leq \frac{1}{N} \text{tr}(\mathbf{K} - \mathbf{L}_m \mathbf{L}_m^\top) \|h\|_{\mathcal{H}_X}^2.$$

From the right-hand side, we infer that the mean-squared error of approximation is controlled by the reduction in the trace error by the low-rank approximation of the kernel matrix  $\mathbf{K}$ . Hence, for any general  $h \in \mathcal{H}_X$ , the pivoting strategy of the pivoted Cholesky of Harbrecht et al. [2012] is the optimal. However, the strategy in Algorithm 4.1 might result in a lower rank for the task at hand. The total cost of performing the  $m$  steps of Algorithm 4.1 is  $\mathcal{O}(m^2 N)$ , see Filipovic et al. [2023].

**4.2. Step 2: Retrieval of probability weights.** Having extracted the set of  $m$  scenarios  $\Xi := \{\xi_1, \dots, \xi_m\} = \{\mathbf{x}_{\pi(1)}, \dots, \mathbf{x}_{\pi(m)}\}$ , we proceed to enforce the probability simplex constraints. We deploy the ADMM algorithm, see Boyd [2011], Parikh [2014]. This approach can be used for projecting least-squares solutions of linear systems onto convex sets. Denote the set of the two simplex constraints as

$$(4.5) \quad \Delta_+ := \{\mathbf{w} \in \mathbb{R}^m : \mathbf{w} \geq \mathbf{0}\}, \quad \Delta_1 := \{\mathbf{w} \in \mathbb{R}^m : \mathbf{1}^\top \mathbf{w} = 1\}.$$

We now use the ADMM algorithm to solve the following problem

$$(4.6) \quad \begin{aligned} \mathbf{\Lambda} &= \underset{\mathbf{w} \in \mathbb{R}^m}{\text{argmin}} \|\mathbf{V}_{2q}^\top(\xi_1, \dots, \xi_m) \mathbf{w} - \hat{\mathbf{y}}\|_2 \\ &\text{subject to: } \Delta := \Delta_+ \cap \Delta_1. \end{aligned}$$

The solution to the above problem gives us the corresponding probabilities  $\lambda_j$  for the scenarios  $\xi_j$  for  $1 \leq j \leq m$ .

The steps for solving the EMP are summarized in Algorithm 4.2

---

**Algorithm 4.2** Final algorithm for scenario representation

---

- input:** set of samples  $X := \{\mathbf{x}_1, \dots, \mathbf{x}_N\}$   
**output:**  $m$  scenarios  $\Xi := \{\xi_1, \dots, \xi_m\} \subset \mathbb{R}^d$  and their probabilities  $\{\lambda_1, \dots, \lambda_m\} \subset \Delta$
- 1: Compute the empirical moment matrix  $\mathbf{M}$ .
  - 2: Perform pivoted Cholesky of  $\mathbf{M}$ , cp.(3.1) to obtain  $\mathbf{B}_M$ .
  - 3: Set  $\mathbf{Q} = \mathbf{V} \mathbf{B}_M / \sqrt{N}$  and perform OMP on  $N \mathbf{Q} \mathbf{Q}^\top$ , cp.(4.1).
  - 4: Extract the scenarios as  $\xi_j = \mathbf{x}_{\pi(j)}$ ,  $1 \leq j \leq m$  ( $\pi$  is the set of pivots obtained from the OMP).
  - 5: Retrieve  $\lambda_j$  by solving (4.6) using ADMM.
- 

**Remark 4.1.** *An extremely popular method to solve least squares problems, that is employed vastly in statistics and compressive sensing is the basis pursuit, i.e.,  $\ell_1$ -regularized least squares, or LASSO. A well-known property of LASSO is that of subset selection i.e., it leads to sparse solutions of least squares problems, see Hastie et al. [2003]. It thus suggests itself as a viable alternative to solving the EMP. However, in our particular setting of finding optimal representation using scenarios, it does not lead to sparsity. Concretely, the minimizer of the basis pursuit problem*

$$\mathbf{w}^* = \underset{\mathbf{w} \in \mathbb{R}^N}{\text{argmin}} \frac{1}{2} \|\mathbf{Q}^\top \mathbf{w} - \tilde{\mathbf{y}}\|_2^2 + \lambda \|\mathbf{w}\|_1 = \underset{\mathbf{w} \in \mathbb{R}^N}{\text{argmin}} \frac{1}{2} \|\mathbf{V}^\top \mathbf{w} - \hat{\mathbf{y}}\|_2^2 + \lambda \|\mathbf{w}\|_1, \lambda > 0,$$

has the constant form  $\mathbf{w}^* = c \mathbf{1}$  with

$$c = \begin{cases} \frac{1-N\lambda}{N}, & \text{if } \frac{1}{N} > \lambda, \\ 0, & \text{otherwise.} \end{cases}$$

*Proof.* We define the two respective cost functions  $g_\lambda, h_\lambda: \mathbb{R}^N \rightarrow \mathbb{R}$  as

$$g_\lambda(\mathbf{w}) := \frac{1}{2} \|\mathbf{Q}^\top \mathbf{w} - \tilde{\mathbf{y}}\|_2^2 + \lambda \|\mathbf{w}\|_1, \quad \text{and} \quad h_\lambda(\mathbf{w}) := \frac{1}{2} \|\mathbf{V}^\top \mathbf{w} - \hat{\mathbf{y}}\|_2^2 + \lambda \|\mathbf{w}\|_1.$$

Clearly, for given  $\lambda > 0$ , both  $g_\lambda$  and  $h_\lambda$  are convex functions. Therefore,  $g_\lambda$  and  $h_\lambda$  are subdifferentiable over  $\mathbb{R}^N$  cp. [Beck, 2017, Corollary 3.15]. We can compute them as, cf. Beck [2017],

$$\partial g_\lambda(\mathbf{w}) = \mathbf{Q}\mathbf{Q}^\top \mathbf{w} - \mathbf{Q}\tilde{\mathbf{y}} + \lambda \partial \|\mathbf{w}\|_1, \text{ and } \partial h_\lambda(\mathbf{w}) = \mathbf{V}\mathbf{V}^\top \left( \mathbf{w} - \frac{1}{N} \mathbf{1} \right) + \lambda \partial \|\mathbf{w}\|_1, \text{ where}$$

$$(\partial \|\mathbf{w}\|_1)_i = \begin{cases} \text{sign } w_i, & w_i \neq 0, \\ x \in [-1, 1], & w_i = 0. \end{cases}$$

From Lemma 3.6, there holds  $\mathbf{Q}\tilde{\mathbf{y}} = \mathbf{Q}\mathbf{Q}^\top \mathbf{1} \frac{1}{N} = \frac{1}{N} \mathbf{1}$ . Hence, the subgradient  $\partial g_\lambda$  reads

$$\partial g_\lambda \left( \frac{c}{N} \mathbf{1} \right) = \left( \frac{c-1}{N} + \lambda \text{sign}(c) \right) \mathbf{1}.$$

Since  $\mathbf{0} \in \partial g_\lambda$  describes the optimality for this strictly convex problem, we can exclude  $c < 0$ , since then the subgradient will be strictly element-wise negative. However, suppose that  $1/N > \lambda$  and  $c > 0$ , then, from the equation  $\frac{c-1}{N} + \lambda \text{sign}(c) = 0$ ,  $c = 1 - N\lambda$  proves to be optimal. For  $1/N \leq \lambda$ , the subgradient evaluated at  $\mathbf{0}$  becomes

$$\partial g_\lambda(\mathbf{0}) = \left( -\frac{1}{N} + \lambda|x| \right) \mathbf{1},$$

where we can again deduce  $\mathbf{0} \in \partial g_\lambda(\mathbf{0})$  with  $x = 1/(N\lambda)$ . For  $h_\lambda$ ,

$$\partial h_\lambda \left( \frac{c}{N} \mathbf{1} \right) = \mathbf{V}\mathbf{V}^\top \left( \frac{c-1}{N} + \lambda \text{sign}(c) \right) \mathbf{1}, \text{ and } \partial h_\lambda(\mathbf{0}) = \mathbf{V}\mathbf{V}^\top \left( -\frac{1}{N} + \lambda|x| \right) \mathbf{1},$$

the cases are analogous. □

*Note that in the above proof, we do not assume any positivity of the weight vector  $\mathbf{w}$ . The result therefore has far-reaching consequences for practical purposes. Foremostly, it shows that it is not possible to obtain optimal quadrature rules (with few atoms) in general that match the empirical moments of polynomials. This fact severely restricts the pool of candidate algorithms that can be deployed for efficient recovery of a few scenarios from the empirical moments. In particular, many popular first-order proximal gradient methods, like the FISTA, see Beck and Teboulle [2009], Nesterov [1983], POGM, see Taylor et al. [2017], Kim and Fessler [2018], etc. to name a few cannot be used in this context.*

## 5. NUMERICAL EXPERIMENTS

In this section, we perform numerical experiments to investigate the behavior of the proposed algorithms concerning the dimension, the number of data points, and the order of the maximum degree of the polynomial basis generating the moment matrix in question. We test the algorithm by Lasserre [2010], the maximum volume algorithm, see Bittante et al. [2016], Bos et al. [2010, 2011], Golub and Van Loan [2013], Sommariva and Vianello [2009], the graded hard thresholding pursuit (GHTP), see Bouchot et al. [2016], the OMP Algorithm 4.1, and finally the covariance scenarios described in Algorithm 2.1. Algorithm 2.1 is only attempted for  $q = 1$  since it was developed solely to match covariance. The flat extensions for Lasserre's algorithm is obtained by a convex relaxation and semidefinite programming (SDP). We start from a rank- $r$  input moment matrix  $\mathbf{M}_{\mathbf{y}} \in \mathbb{R}^{m_q \times m_q}$  with the goal to find its flat extension  $\mathbf{M}_{\tilde{\mathbf{y}}} \in \mathbb{R}^{m_{q+l} \times m_{q+l}}$  for some  $l \geq 1$ . Given the block matrix representation

$$\mathbf{M}_{\tilde{\mathbf{y}}} = \begin{bmatrix} \mathbf{A}_{\tilde{\mathbf{y}}} & \mathbf{B}_{\tilde{\mathbf{y}}} \\ \mathbf{B}_{\tilde{\mathbf{y}}}^\top & \mathbf{C}_{\tilde{\mathbf{y}}} \end{bmatrix}$$

with

$$\mathbf{A}_{\tilde{\mathbf{y}}} \in \mathbb{R}^{m_{q+l-1} \times m_{q+l-1}}, \mathbf{B}_{\tilde{\mathbf{y}}} \in \mathbb{R}^{m_{q+l-1} \times (m_{q+l} - m_{q+l-1})}, \mathbf{C}_{\tilde{\mathbf{y}}} \in \mathbb{R}^{(m_{q+l} - m_{q+l-1}) \times (m_{q+l} - m_{q+l-1})},$$

we subsequently minimize the trace of the bottom-right block. If now flat extension is found, we increase  $l$  and restart the procedure.

All algorithms have been implemented on a single Intel Xeon E5-2560 core with 3 GB of RAM, except for Lasserre's algorithm which is run on an 18-core Intel i9-10980XE machine with 64 GB RAM.

**5.1. Multivariate Gaussian mixture distributions.** We first examine the different algorithms on simulated data sampled from a Gaussian mixture model with different numbers of dimensions  $d$  and

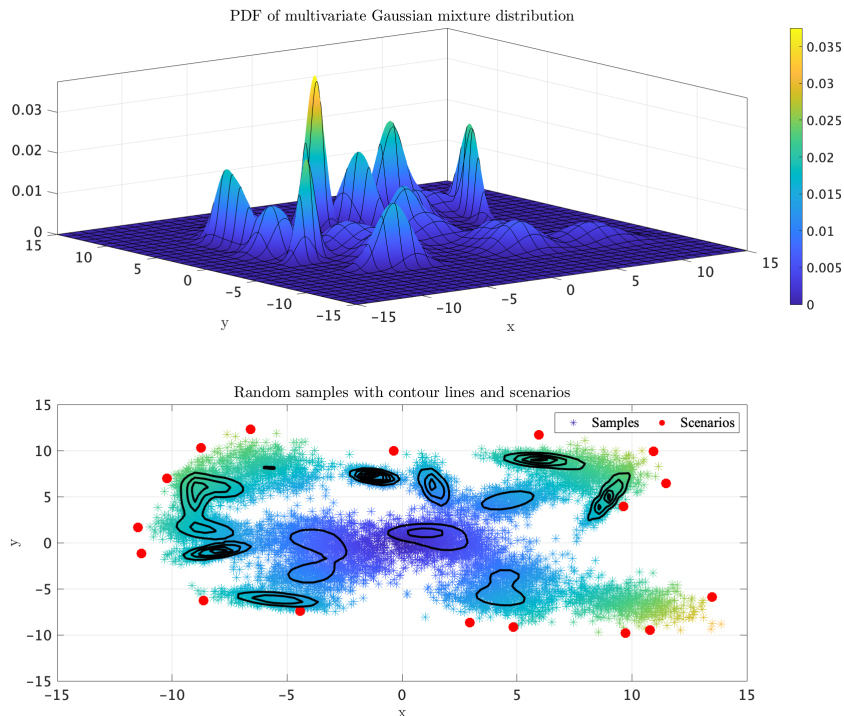


FIGURE 1. The OMP scenarios (red dots) from 10000 random samples of a bivariate Gaussian mixture distribution with their contour lines. The PDF of the distribution is given in the first tile.

having different numbers of clusters  $c$ , components of the mixture distribution, that induce multiple modes into the joint distribution. We test for  $d = 2, 5, 10, 20, 50, 100$  and  $c = 5, 10, 20, 25, 50, 100, 150, 200$ . To investigate the efficacy of the algorithms, we do not use a higher  $c$  for relatively lower  $d$  and vice-versa. The means of the different clusters are taken to be random vectors of uniformly distributed numbers in the interval  $(-50, 50)$ . The variance-covariance matrices for the different clusters are either (i) randomly generated positive definite matrices with  $\mathcal{N}(1, 1)$ -distributed eigenvalues, or (ii) the identity matrix. Except in the case of unit variance-covariance, the different clusters have different variance-covariance matrices. The mixing proportions for the different clusters are taken to be either (i) random or, (ii) equal. We can categorize them as

- (1) random variance-covariance and random mixing proportion
- (2) random variance-covariance and equal mixing proportion
- (3) unit variance-covariance and random mixing proportion
- (4) unit variance-covariance and equal mixing proportion

For each of the above cases, 100 data sets are randomly constructed, each containing 10000 samples. For each data set containing the samples, we calculate the sample moments  $\hat{\mathbf{y}}$  up to order  $2q$  with  $q = 1, 2$  which give rise to the empirical moment matrices  $\mathbf{M}_{\hat{\mathbf{y}}}$  of orders 1 and 2 respectively. The 100-dimensional and 50-dimensional data sets are computed for  $q = 1$  only, still resulting in 5151-dimensional, and 1326-dimensional moment matrices, respectively. The biggest moment matrix for  $q = 2$  is computed for twenty dimensions, resulting in a 10262-dimensional moment matrix. It is noteworthy to point out that there is, theoretically speaking, no bound on the degree to which we can calculate the moments. However, the computational cost of obtaining higher-order moment information is high. We provide a visualization for the case  $d = 2$  where we first generate 10000 random samples from a bivariate Gaussian mixture distribution with 20 clusters, and then retrieve the OMP scenarios as in Figure 1.

We compare the performance of the different algorithms with respect to the relative errors, computation times, and the number of scenarios extracted, across different dimensions and clusters, as shown subsequently.

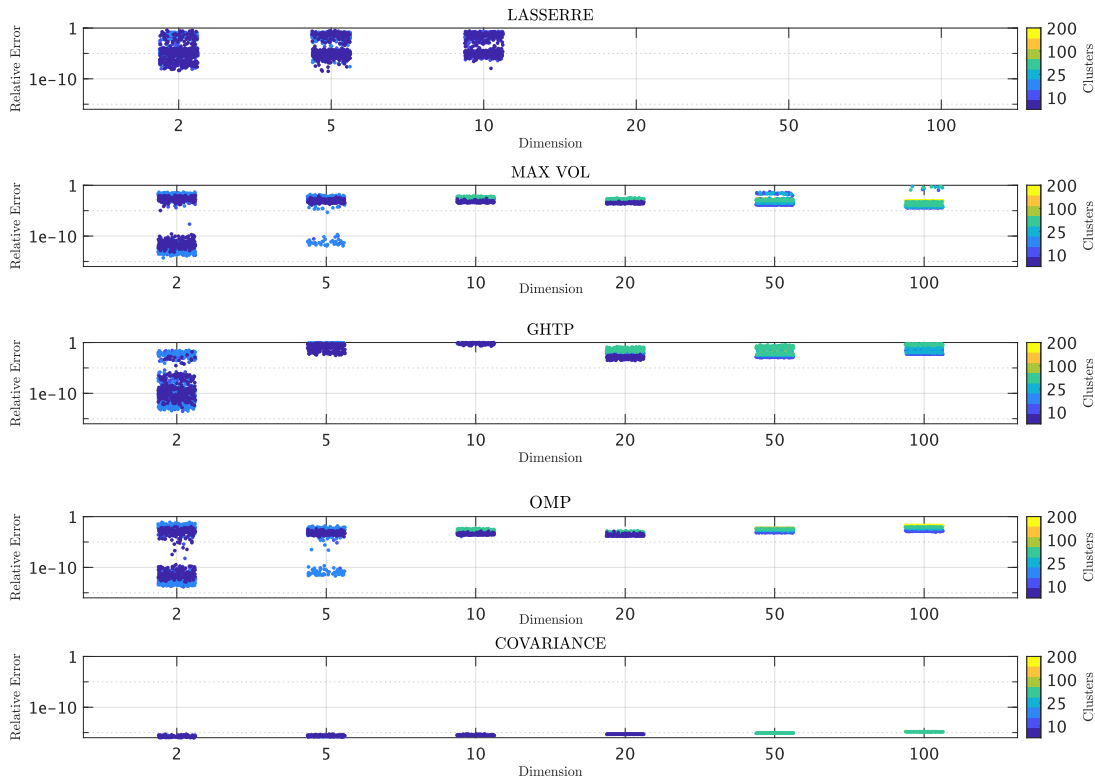


FIGURE 2. Relative error comparison for  $q = 1$ . The data are generated from Gaussian mixture models according to Section 5.1. The relative errors (left  $y$ -axis) are computed according to (5.1). The  $x$ -axis shows the dimension  $d$  and the right  $y$ -axis shows the number of clusters entering the mixture distribution.

5.1.1. *Relative errors.* We compare the behavior of the different algorithms about how well the sample moments are matched using the scenarios. For a fair comparison of the relative errors for the different algorithms, we define

$$(5.1) \quad \text{err} := \frac{\|M_{\hat{y}} - V^\top \Lambda V\|_F}{\|M_{\hat{y}}\|_F}$$

where  $V$  is the Vandermonde matrix of order  $q$  generated from the samples, and  $\Lambda$  is the (sparse) diagonal matrix containing the respective probability weights of the samples.

We plot the relative errors (5.1) against the dimensions and number of clusters in Figure 2 and Figure 3 respectively for  $q = 1$  and  $q = 2$ . In both figures, the  $y$ -axis represents the relative error in the log scale. The  $x$ -axis contains the different dimensions  $d$  which is a categorical variable. The color bar depicts the different number of clusters and is taken as a categorical variable. The performance of the different algorithms is shown in the respective tiles.

*Lasserre.* The algorithm from Lasserre [2010] is computationally feasible only until dimension 10 for  $q = 1$  and  $d = 5$  for  $q = 2$ . It breaks down thereafter since the algorithm involves finding flat extensions requiring the solution of large semidefinite relaxations. For each dimension, the relative errors vary considerably from the order of  $10^{-8}$  to  $10^{-1}$  for  $q = 1$ , and  $10^{-6}$  to  $10^{-1}$  for  $q = 2$ . There is no particular pattern in their distribution with the number of clusters. The results suggest that Lasserre’s algorithm is not well suited for large and high-dimensional data sets.

*Maximum volume.* We find that, unlike Lasserre’s algorithm, the maximum volume algorithm is applicable up to  $d = 100$  for  $q = 1$ , and  $d = 20$  for  $q = 2$ . The relative errors range from the order of  $10^{-14}$  to  $10^{-2}$  for  $q = 1$ , and  $10^{-4}$  to  $10^{-3}$  for  $q = 2$ . They exhibit a slight decrease with the number of dimensions, but across dimensions, and a maximum increase by a factor of 10 with the number of clusters. This is a considerable improvement from Lasserre’s algorithm insofar as the relative errors are more stable across

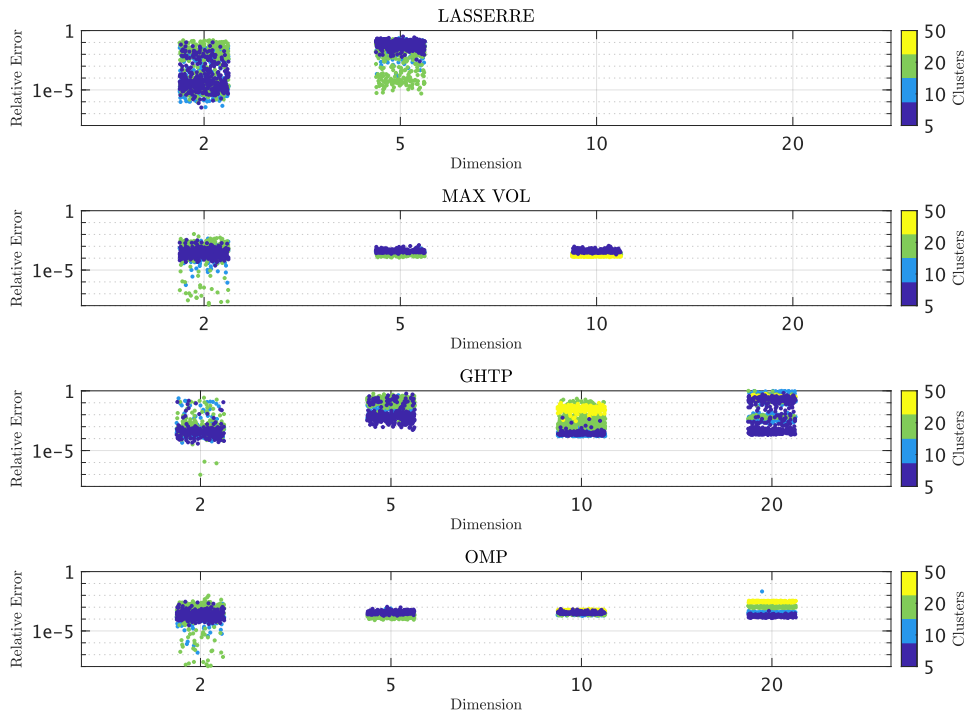


FIGURE 3. Relative error comparison for  $q = 2$ . The data are generated from Gaussian mixture models according to Section 5.1. The relative errors (left  $y$ -axis) are computed according to (5.1). The  $x$ -axis shows the dimension  $d$  and the right  $y$ -axis shows the number of clusters entering the mixture distribution.

dimensions and the number of clusters. However,  $d = 20$  and  $q = 2$  exhibit a sharp decrease and range in the order of  $10^{-10}$ , however.

GHTP. This algorithm is easily applicable up to  $d = 100$  for  $q = 1$ , and  $d = 20$  for  $q = 2$ . The relative errors range from the order of  $10^{-13}$  to  $10^0$  for  $q = 1$ . Except for the case of  $d = 2$ , the relative errors mostly range from the order of  $10^{-4}$  to  $10^0$ . For  $q = 2$ , the relative errors range from the order of  $10^{-4}$  to  $10^0$ . In terms of the stability of the relative errors, although the GHTP fares better than the maximum volume algorithm, it is a deterioration when considering the range of the errors.

OMP. We find that this algorithm is easily applicable until  $d = 100$  for  $q = 1$ , and  $d = 20$  for  $q = 2$ . The relative errors range from the order of  $10^{-14}$  to  $10^{-2}$  for  $q = 1$ , and  $10^{-10}$  to  $10^{-3}$  for  $q = 2$ , with most in the range of  $10^{-4}$  to  $10^{-3}$ . Not only are the errors overall much more stable across the different dimensions, but their orders are also comparable to that of the maximum volume algorithm. Except for the case of  $d = 2$ , the relative errors mostly range from the order of  $10^{-4}$  to  $10^{-2}$ . While the range of the relative errors for the OMP is similar to that of the maximum volume algorithm, there is a difference in that we do not observe any significant noticeable pattern in the distribution of the relative errors across dimensions.

Covariance scenarios. We find that this algorithm is not only applicable until  $d = 100$ , but the relative errors are considerably smaller than for all the above algorithms, ranging in the order of  $10^{-17}$  to  $10^{-15}$ . Hence, as stipulated in the earlier section, in the special case of covariance matrices, i.e., when  $q = 1$ , the covariance algorithm performs the best since it matches exactly all the sample moments until the second moment. By its construction, covariance scenarios are not applicable for  $q = 2$ .

5.1.2. *Number of scenarios.* For practical purposes when working with large data sets, given a relative error, sparsity is preferred in the number of scenarios extracted when solving the EMP. To that end, we compare the number of scenarios extracted from the different algorithms. Except for the case of covariance scenarios, that have uniform weights, for the remaining methods, we retrieve the weights using the ADMM algorithm described in Section 4.2.

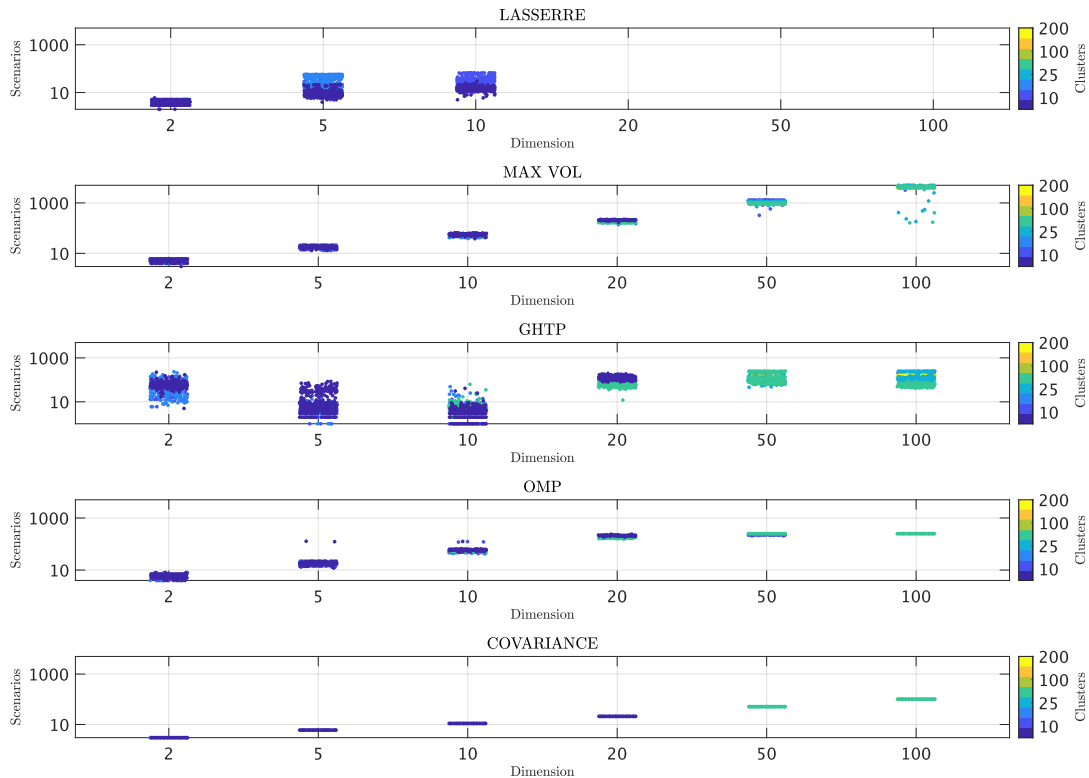


FIGURE 4. Number of scenarios comparison for  $q = 1$ . The data are generated from Gaussian mixture models according to Section 5.1. The left  $y$ -axis shows the number of scenarios. The  $x$ -axis shows the dimension  $d$  and the right  $y$ -axis shows the number of clusters entering the mixture distribution.

For each probability vector, we set the entries less than  $10^{-8}$  to zero. As such, we consider the number of scenarios to be the number of non-zero entries of the modified probability vector. We then plot the number of scenarios against the dimensions and number of clusters for  $q = 1, 2$  in Figure 4 and Figure 5 respectively. In both figures, the  $y$ -axis denotes the number of scenarios and is taken in the log scale. The  $x$ -axis contains the different dimensions which is a categorical variable. The color bar denotes the number of clusters, and it is also taken as a categorical variable. The performance of the different algorithms is shown in the respective tiles.

**Lasserre.** Lasserre’s algorithm depends on the flat extension of the moment matrix, with the precise rank of the flat extension determining the number of scenarios. Accordingly, we find that the number of scenarios, while not too high for each dimension, still shows variability for  $d = 5, 10$ . For  $q = 2$ , the number of scenarios is also not exceedingly high.

**Maximum volume.** We first observe that the number of scenarios is considerably high across the dimensions, ranging from 4000 to 5000 for  $d = 100$ . Except for  $d = 100$ , there is no considerable difference in the number of scenarios retrieved with the number of clusters. Similar to the case for  $q = 1$ , the number of scenarios is considerably high across the dimensions and is equal to 10000 for  $d = 20$ , i.e., it does not give sparse scenarios and considers all the sample points. There is also no variation with different clusters for either dimension. Nevertheless, it cannot be used for sparse recovery of scenarios from large samples.

**GHTP.** For this algorithm, we find that the number of scenarios is much less compared to that of the maximum volume algorithm, and similar to that of Lasserre’s algorithm for  $d = 2, 5, 10$ . This result is not surprising, given that the algorithm constructs the index set whose size equals a prior input maximum number of iterations (see Bouchot et al. [2016]). For  $d = 20, 50, 100$ , however, the number of scenarios varies considerably with the number of clusters. For  $q = 2$ , the number of scenarios is much less, with the maximum being 250, compared to that of the maximum volume algorithm, nevertheless, it varies considerably with the number of clusters for each dimension.



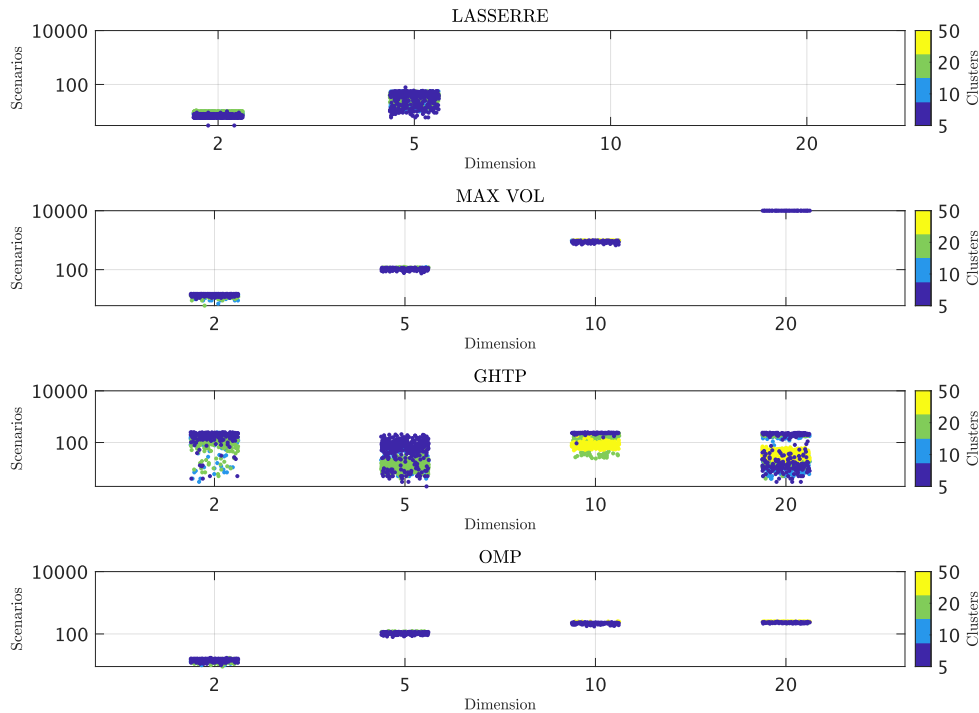


FIGURE 5. Number of scenarios comparison for  $q = 2$ . The data are generated from Gaussian mixture models according to Section 5.1. The left  $y$ -axis shows the number of scenarios. The  $x$ -axis shows the dimension  $d$  and the right  $y$ -axis shows the number of clusters entering the mixture distribution.

OMP. The number of scenarios retrieved is somewhat similar to that of the GHTP. This results from the fact that we set the maximum number of iterations for the OMP to be the same as that of the GHTP. Unlike the GHTP however, we find that in this case, there is no considerable variation in the number of scenarios with the number of clusters, for each dimension. Therefore, the OMP outperforms the above algorithms, with regard to the number as well as the consistency in the retrieval of scenarios. The same interpretation holds for  $q = 2$ .

Covariance scenarios. The range for the number of scenarios is the least among all the algorithms for all the dimensions. Furthermore, there is no variation in the case of the different clusters for each dimension. This reaffirms that the covariance scenarios perform the best about the number of scenarios retrieved, keeping in mind that they are applicable only in the case  $q = 1$ .

5.1.3. *Computation time.* Finally, we test how fast the algorithms are in computing the scenarios from large empirical data sets, keeping practical applications in mind. To that end, we plot the CPU run times of the different algorithms against the different dimensions and number of clusters for  $q = 1, 2$  in Figure 6 and Figure 7 respectively. We take the  $y$ -axis to be the computation times in the log scale. The  $x$ -axis contains the different dimensions, which is a categorical variable. The color bar depicts the different number of clusters and is also taken as a categorical variable.

Lasserre. Computation times range from  $10^{-1}$  to  $10^3$  seconds just the until  $d = 10$  only. For  $d = 5$ , the run times increase with the number of clusters, by an order of 10. Therefore, Lasserre's algorithm becomes computationally costly in the face of higher dimensions. For  $q = 2$ , We find that the times range from  $10^{-1}$  to  $10^3$  seconds until  $d = 5$  only. For  $d = 5$ , the run times increase with the number of clusters, by an order of 100.

Maximum volume. The run times range from  $10^{-2}$  to  $10^3$  seconds across the different dimensions and clusters. A noticeable aspect of this algorithm is that while the run-time increases, the variation among them, however, decreases with an increase in the dimension. For  $q = 2$ , the run times range from  $10^{-1}$  to  $10^3$  seconds. Similar to  $q = 1$ , the run times of the algorithm for this case increase, and the variation

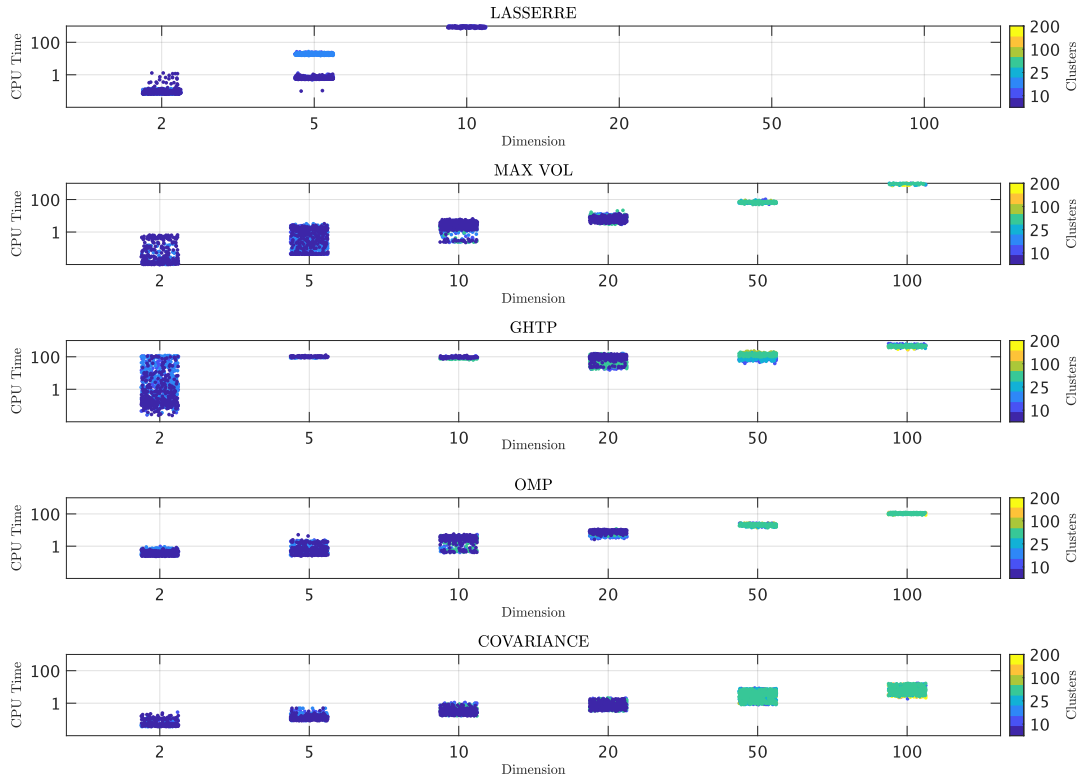


FIGURE 6. Computation time comparison for  $q = 1$ . The data are generated from Gaussian mixture models according to Section 5.1. The left  $y$ -axis shows the computation time. The  $x$ -axis shows the dimension  $d$ , and the right  $y$ -axis shows the number of clusters entering the mixture distribution.

among them, decreases with an increase in the dimension. However, a particular drawback remains that the run times show sharp increases with the number of dimensions.

GHTP. For the GHTP algorithm, the times range from  $10^{-1}$  to  $10^2$  seconds. Except for the case of  $d = 2$ , overall the run times of the GHTP algorithm lie in the range of  $10^2$ , i.e., it is fairly similar across the different dimensions and clusters and does not increase with an increase in either. For  $q = 2$ , the times range from  $10^2$  to  $10^3$  seconds. Unlike in the case for  $q = 1$ , here, we observe that in general, the times increase with the number of dimensions, with a sharp increase for  $d = 20$ .

OMP. The run times of the OMP range from  $10^{-1}$  to  $10^2$  seconds across different dimensions and clusters. Similar to the maximum volume algorithm, the OMP also shows a gradual increase in the computation times with an increase in the dimensions. Moreover, in general, it fares better than the GHTP, whose run time is at least higher by a factor of 10. For  $q = 2$ , we observe that the run times range from  $10^{-1}$  to  $10^2$  seconds. Despite the increase in the run times with the number of dimensions, nevertheless, we can conclude that it is still considerably faster than all of the above algorithms. Note that except for  $d = 20$  for all the other dimensions, it is still below 10 seconds, which further reinforces the efficiency of the algorithm.

Covariance scenarios. We see that the run times for the covariance scenarios range from  $10^{-2}$  to  $10^1$  seconds, which is considerably better than that of all the above algorithms.

**5.2. Portfolio optimization with CVaR constraints.** In this section, we discuss an application of the proposed OMP algorithm in finance using excess return data from [Fama-French](#). The data set contains more than 25000 daily excess returns of 25 financial assets. A portfolio, or trading strategy, is defined through the number and choice of assets. An important aspect of portfolio risk management is to address extreme outcomes, wherein investors are concerned by the multivariate nature of risk and the scale of the portfolios under consideration. For decision-making, any sensible strategy involves dimension reduction

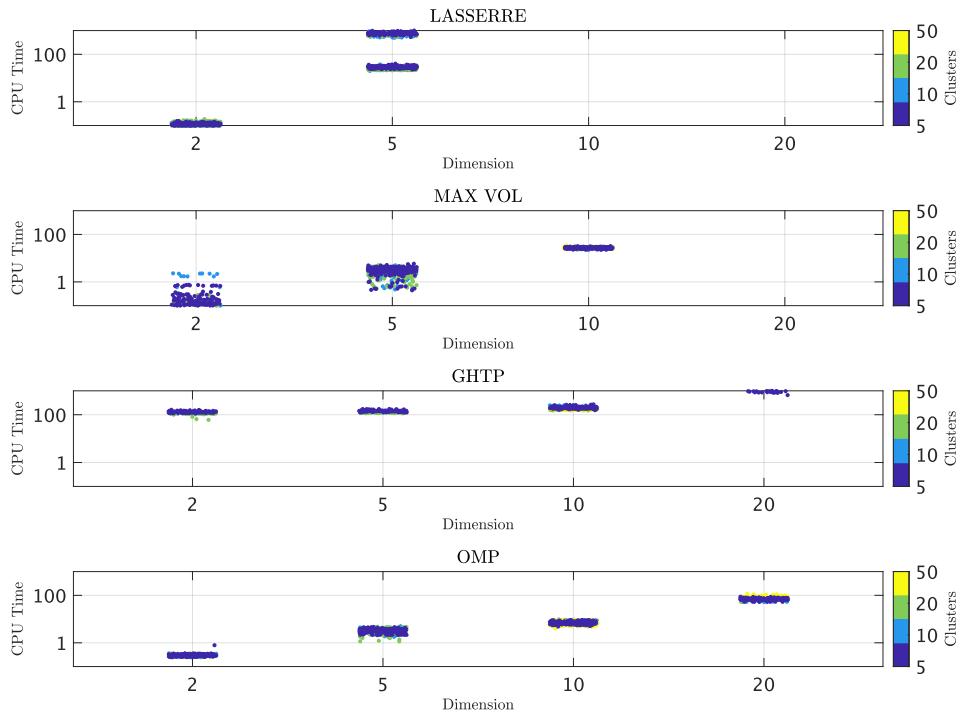


FIGURE 7. Computation time comparison for  $q = 2$ . The data are generated from Gaussian mixture models according to Section 5.1. The left  $y$ -axis shows the computation time. The  $x$ -axis shows the dimension  $d$ , and the right  $y$ -axis shows the number of clusters entering the mixture distribution.

and modeling the key features of the overall risk landscape. To this end, we consider here the problem of maximizing expected portfolio returns with expected shortfall constraints as a proxy for the entailing risk. Expected shortfall, also known as conditional value-at-risk (CVaR), is a coherent risk measure that quantifies the tail risk an investment portfolio has, see [McNeil et al. \[2015\]](#). In 2016, the [Basel committee](#) hosted by the Bank of International Settlements (BIS) proposed an internationally agreed set of regulatory measures in response to the financial crisis of 2007-2009; one of them was that the market risk capital of banks should be calculated with CVaR or expected shortfall, see [Basel Committee on Banking Supervision \(BCBS\) \[2019\]](#). Nevertheless, methods for portfolio optimization that rely on such a downside risk measure as CVaR, are often difficult to implement, do not scale efficiently, and may result in less-than-ideal portfolio allocations. To resolve these issues and construct an optimal portfolio that minimizes shortfall risk, we consider the following optimization problem:

$$(5.2) \quad \begin{aligned} \mathbf{w}^* &= \underset{\mathbf{w} \in \mathbb{R}^d}{\operatorname{argmin}} && -\mathbf{w}^\top \boldsymbol{\mu} \\ &\text{subject to: } && \operatorname{CVaR}_\alpha \leq \delta, \quad \mathbf{w} \in W, \end{aligned}$$

where  $\boldsymbol{\mu}$  is the expected return of the individual assets,  $\operatorname{CVaR}_\alpha$  denotes the conditional value-at-risk, at the  $\alpha$  level with  $\alpha \in (0, 1)$ , and  $\delta$  represents the maximum portfolio loss that is acceptable. Specifically, the CVaR or expected shortfall is the expected loss conditional on the event that the loss exceeds the quantile associated with the probability  $\alpha$ . Further,  $W$  can capture constraints like relative portfolio weights, short-sale restrictions, limits on investment in a particular asset, etc.

We use the reformulation of the CVaR as in [Uryasev and Rockafellar \[2001\]](#) to find a global solution. While, generally for the optimization approach to work, simulations using a Monte-Carlo approach or bootstrapping of historical data are required, we use our generated scenarios, using the OMP, to showcase the applicability in the case of non-smooth optimization as well. The scenarios from the OMP capture the underlying tail risk, which leads to efficient portfolios whose risk lies below a certain threshold. To that end, we split the portfolio data set into a training set of 10000 observations and a testing set of the rest of the observations. We first extract the scenarios and the corresponding probabilities from the

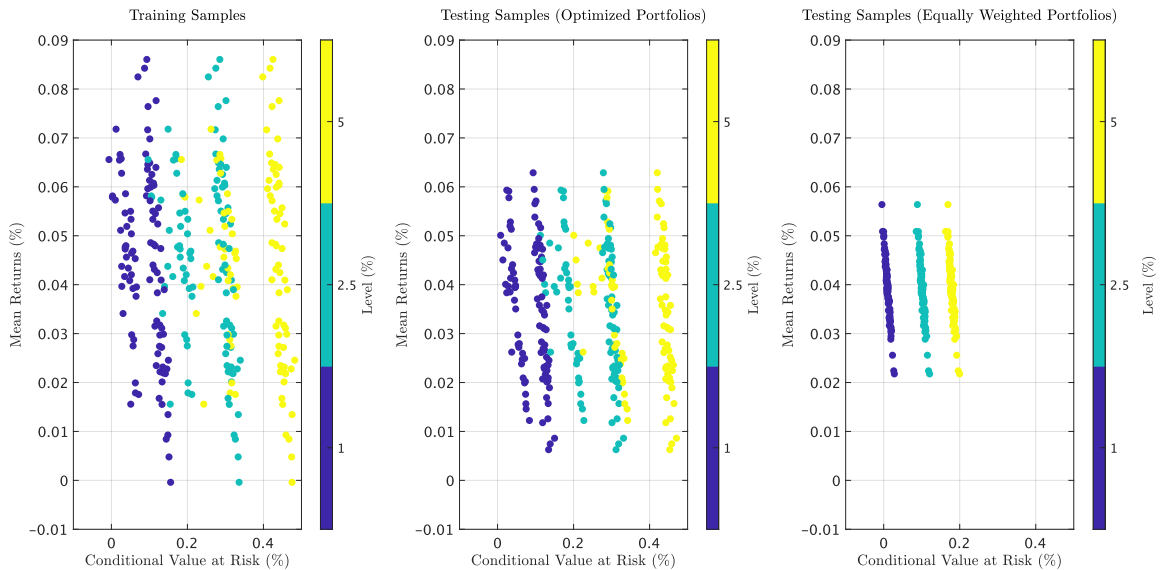


FIGURE 8. Daily mean returns versus CVaR for the worst 1%, 2.5% and 5% cases of the expected portfolio loss applied to the training and testing samples with both optimized portfolios and the naive portfolio. The data are daily returns from the 25-dimensional Fama-French portfolios.

training data set using the OMP algorithm, see Algorithm 4.1. We then solve problem (5.2) using the scenarios and the approach suggested in Uryasev and Rockafellar [2001], taking  $\delta$  to be the conditional value-at-risk for the naive portfolio rule  $\mathbf{w} = (1/d)\mathbf{1}$  at the confidence levels  $\alpha = 0.95, 0.975, 0.99$ , which correspond to the expected loss in the worst 5%, 2.5% and 1% cases respectively. The  $\text{CVaR}_\alpha$  in the constraint is the corresponding conditional value-at-risk of the expected portfolio loss in the worst 5%, 2.5% and 1% case as well. We perform back-testing using the optimized portfolio weights on the test sample observations. We perform 100 simulations and observe the distribution of the expected daily returns versus the CVaR or the expected shortfall for both the training and testing samples in Figure 8. Furthermore, we plot the same for the case of the equally weighted portfolios. All the observations are considered as percentages, the color bar indicates the  $\alpha$  level considered for the optimization problem. The figure shows that the optimized portfolios perform well on the testing set as well, achieving a yearly mean return of about 12% to 14% in general; hence, our realized scenarios can still capture the behavior of the underlying asset returns considerably well, even when trying to match moments of non-smooth functions of polynomials.

## 6. CONCLUSION AND FUTURE WORK

We have proposed two algorithms to find scenarios representing large samples of panel data. The first converts estimated sample covariance matrices to a set of uniformly distributed scenarios that possibly have not been observed before. The second picks a particular subset of realized data points, considering higher-order moment information present in the sample.

The numerical studies suggest that both algorithms perform well with respect to computational efficiency and accuracy relative to extant proposals, such as the maximum volume approach by Bittante et al. [2016], greedy hard thresholding, and Lasserre [2010] multivariate Gaussian quadrature in particular in higher dimensions.

Our framework allows for extensions with non-uniform weighting of the sample points, and expectations of a bigger class of functions rather than just polynomials. We expect this to be beneficial for non-smooth scenario-based problems as well.

## REFERENCES

- Caio Almeida and René Garcia. Economic implications of nonlinear pricing kernels. *Management Science*, 63(10):3361–3380, 2017.
- Caio Almeida, Gustavo Freire, René Garcia, and Rodrigo Hizmeri. Tail risk and asset prices in the short-term. *SSRN Electronic Journal*, 2022.
- Francis Bach. On the Equivalence between Kernel Quadrature Rules and Random Feature Expansions. *Journal of Machine Learning Research*, 18(21):714–751, 2017.
- Basel Committee on Banking Supervision (BCBS). Minimum capital requirements for market risk, 2019.
- Christian Bayer and Josef Teichmann. The proof of Tchakaloff’s theorem. *Proceedings of the American Mathematical Society*, 134(10):3035–3040, 2006.
- Amir Beck. *First-Order Methods in Optimization*. Society for Industrial and Applied Mathematics, 2017.
- Amir Beck and Marc Teboulle. A fast iterative shrinkage-thresholding algorithm for linear inverse problems. *SIAM Journal on Imaging Sciences*, 2(1):183–202, 2009.
- Ayoub Belhadji, Rémi Bardenet, and Pierre Chainais. Kernel quadrature with DPPs. In *Proceedings of the 33rd International Conference on Neural Information Processing Systems*. Curran Associates Inc., 2019.
- Alain Berlinet and Christine Thomas-Agnan. *Reproducing kernel Hilbert spaces in probability and statistics*. Springer Science & Business Media, 2011.
- Claudia Bittante, Stefano De Marchi, and Giacomo Elefante. A new quasi-Monte Carlo technique based on nonnegative least squares and approximate Fekete points. *Numerical Mathematics: Theory, Methods and Applications*, 9(4):640–663, 2016.
- L. Bos, S. De Marchi, A. Sommariva, and M. Vianello. Computing multivariate Fekete and Leja points by numerical linear algebra. *SIAM Journal on Numerical Analysis*, 48(5):1984–1999, 2010.
- Len Bos, Stefano De Marchi, Alvise Sommariva, and Marco Vianello. Weakly admissible meshes and discrete extremal sets. *Numerical Mathematics: Theory, Methods and Applications*, 4(1):1–12, 2011.
- Jean-Luc Bouchot, Simon Foucart, and Pawel Hitczenko. Hard thresholding pursuit algorithms: Number of iterations. *Applied and Computational Harmonic Analysis*, 41(2):412–435, 2016.
- Stephen Boyd. Distributed optimization and statistical learning via the alternating direction method of multipliers. *Foundations and Trends® in Machine Learning*, 3(1):1–122, 2011.
- Francesco Cosentino, Harald Oberhauser, and Alessandro Abate. A randomized algorithm to reduce the support of discrete measures. In *Proceedings of the 34th International Conference on Neural Information Processing Systems*. Curran Associates Inc., 2020.
- Raul Curto and Lawrence Fialkow. *Solution of the truncated complex moment problem for flat data*, volume 568. American Mathematical Society (AMS), 1996.
- Raúl E. Curto and Lawrence A. Fialkow. A duality proof of Tchakaloff’s theorem. *Journal of Mathematical Analysis and Applications*, 269(2):519–532, 2002.
- Stefano De Marchi and Robert Schaback. Stability of kernel-based interpolation. *Advances in Computational Mathematics*, 32(2):155–161, 2010.

- Robert Engle, Guillaume Roussellet, and Emil Siriwardane. Scenario generation for long run interest rate risk assessment. *Journal of Econometrics*, 201(2):333–347, 2017.
- Gregory E Fasshauer. *Meshfree Approximation Methods with Matlab*. World Scientific, 2007.
- Dan Feldman, Melanie Schmidt, and Christian Sohler. Turning Big Data Into Tiny Data: Constant-Size Coresets for  $k$ -Means, PCA, and Projective Clustering. *SIAM Journal on Computing*, 49(3):601–657, 2020.
- Larence A. Fialkow. Minimal representing measures arising from rank-increasing moment matrix extensions. *Journal of Operator Theory*, 42(2):425–436, 1999.
- Damir Filipovic, Michael Multerer, and Paul Schneider. Adaptive joint distribution learning, 2023.
- S. Foucart and H. Rauhut. *A Mathematical Introduction to Compressive Sensing*. Applied and Numerical Harmonic Analysis. Springer New York, 2013.
- Valentina Ghidini, Michael Multerer, Jacopo Quizi, and Rohan Sen. Observation-specific explanations through scattered data approximation, 2024.
- Gene H. Golub and Charles F. Van Loan. *Matrix Computations*. Johns Hopkins University Press, Baltimore, 4 edition, 2013.
- H. Harbrecht, M. Peters, and R. Schneider. On the low-rank approximation by the pivoted Cholesky decomposition. *Applied Numerical Mathematics*, 62(4):28–440, 2012.
- T. Hastie, R. Tibshirani, and J. H. Friedman. *The Elements of Statistical Learning*. Springer, 2003.
- Satoshi Hayakawa, Harald Oberhauser, and Terry Lyons. Positively weighted kernel quadrature via subsampling. In *Proceedings of the 36th International Conference on Neural Information Processing Systems*. Curran Associates Inc., 2022.
- J. William Helton and Jiawang Nie. A semidefinite approach for truncated  $k$ -moment problems. *Foundations of Computational Mathematics*, 12(6):851–881, 2012.
- Alston S. Householder. *The Theory of Matrices in Numerical Analysis*. Blaisdell Publishing Company, 1965.
- Jonathan Huggins, Trevor Campbell, and Tamara Broderick. Coresets for scalable Bayesian logistic regression. In *Advances in Neural Information Processing Systems 29 (NIPS 2016)*, 2016.
- Donghwan Kim and Jeffrey A. Fessler. Adaptive restart of the optimized gradient method for convex optimization. *Journal of Optimization Theory and Applications*, 178(1):240–263, 2018.
- Stefan Kunis, Thomas Peter, Tim Römer, and Ulrich von der Ohe. A multivariate generalization of Prony’s method. *Linear Algebra and its Applications*, 490:31–47, 2016.
- Jean Bernard Lasserre. *Moments, Positive Polynomials and Their Applications*. Imperial College Press, 2010.
- Monique Laurent. Sums of squares, moment matrices and optimization over polynomials. In *Emerging Applications of Algebraic Geometry*, pages 155–270. Springer Verlag, 2009.
- Alexander J. McNeil, Rüdiger Frey, and Paul Embrechts. *Quantitative Risk Management: Concepts, Techniques and Tools Revised edition*. Number 10496 in Economics Books. Princeton University Press, 2015.

- Yurii Nesterov. A method for unconstrained convex minimization problem with the rate of convergence  $O(1/k^2)$ . *Rossiiskaya Akademiya Nauk*, 269(3):543, 1983.
- Jens Oettershagen. *Construction of Optimal Cubature Algorithms with Applications to Econometrics and Uncertainty Quantification*. PhD dissertation, Rheinischen Friedrich-Wilhelms-Universität Bonn, 2017.
- Neal Parikh. Proximal algorithms. *Foundations and Trends<sup>®</sup> in Optimization*, 1(3):127–239, 2014.
- Vern I. Paulsen and Mrinal Raghupathi. *An introduction to the theory of reproducing kernel Hilbert spaces*, volume 152 of *Cambridge Studies in Advanced Mathematics*. Cambridge University Press, 2016.
- Maryam Pazouki and Robert Schaback. Bases for kernel-based spaces. *Journal of Computational and Applied Mathematics*, 236(4):575–588, 2011.
- Ernest K. Ryu and Stephen P. Boyd. Extensions of Gauss quadrature via linear programming. *Foundations of Computational Mathematics*, 15(4):953–971, 2014.
- Konrad Schmüdgen. *The Moment Problem*. Graduate Texts in Mathematics. Springer International Publishing, 2017.
- Paul Schneider and Fabio Trojani. Fear trading. *SSRN Electronic Journal*, 2015.
- Alvise Sommariva and Marco Vianello. Computing approximate Fekete points by QR factorizations of Vandermonde matrices. *Computers & Mathematics with Applications*, 57(8):1324–1336, 2009.
- Adrien B. Taylor, Julien M. Hendrickx, and François Glineur. Exact worst-case performance of first-order methods for composite convex optimization. *SIAM Journal on Optimization*, 27(3):1283–1313, 2017.
- Stanislav Uryasev and R. Tyrrell Rockafellar. Conditional value-at-risk: Optimization approach. In *Stochastic Optimization: Algorithms and Applications*, page 411–435. Springer US, 2001.
- Holger Wendland. *Scattered data approximation*, volume 17 of *Cambridge Monographs on Applied and Computational Mathematics*. Cambridge University Press, Cambridge, 2005.
- Yuan Xu. *Common zeros of polynomials in several variables and higher dimensional quadrature*. Chapman and Hall/CRC, 1994.
- MICHAEL MULTERER, EULER INSTITUTE, USI LUGANO, VIA LA SANTA 1, 6962 LUGANO, SVIZZERA.  
*Email address:* michael.multerer@usi.ch
- PAUL SCHNEIDER, USI LUGANO AND SFI, VIA BUFFI 6, 6900 LUGANO, SVIZZERA.  
*Email address:* paul.schneider@usi.ch
- ROHAN SEN, EULER INSTITUTE, USI LUGANO, VIA LA SANTA 1, 6962 LUGANO, SVIZZERA.  
*Email address:* rohan.sen@usi.ch